



Magnetic Excitations in Quantum Rare Earth Pyrochlores

by

© Ibsal A T Assi

A thesis submitted to the School of Graduate Studies in partial fulfillment of the requirements for the degree of Master of Science.

Department of Physics and Physical Oceanography
Memorial University

September 2019

St. John's, Newfoundland and Labrador, Canada

Abstract

Rare-earth pyrochlores are materials with chemical formula $A_2B_2O_7$, where A is the rare-earth ion and B is a transition metal. At low temperature, these systems host various magnetic states such as spin ice, spin liquid state, ferromagnetic ordering, all in-all out, and anti-ferromagnetic ordering. For each rare-earth ion with total angular momentum J , the $2J + 1$ fold degeneracy splits into singlets and doublets due to the crystal electric field. However, the crystal electric field ground state for most of the magnetic ions is a doublet that comes into three different varieties, labeled as Γ_3 , Γ_4 , and $\Gamma_{5,6}$. This work focuses only on systems in which the ground state doublet is well-separated from the first excited state so that we end up with effective two-state systems, referred to as quantum rare-earth pyrochlores. The low temperature excitations of interacting spins have a wave nature and are referred to as spin waves or magnons, where the energy of these waves is quantized. To study these magnons, we apply the Holstein-Primakoff transformation on the effective spin Hamiltonian to construct a bosonic Hamiltonian that describes magnons. In this study, we limit ourselves to the linear spin-wave approximation in which we diagonalize the magnonic Hamiltonian analytically and numerically for various systems of interest. In particular, we study magnons in $Nd_2Zr_2O_7$ which orders in an all in-all out state near 0.285 K, in $Er_2Ti_2O_7$ with a antiferromagnetic state below 1.2 K, and finally the $Yb_2Ti_2O_7$ which orders ferromagnetically near 0.2 K.

This work is dedicated to my family and friends for their continuous support

Acknowledgements

First of all, I would like to thank Dr. S. H. Curnoe for her advise and supervision during the production of this work. This work was supported by NSERC.

Table of contents

Title page	i
Abstract	ii
Acknowledgements	iv
Table of contents	v
List of tables	viii
List of figures	x
List of symbols	xiii
List of abbreviations	xiv
1 Introduction	1
1.1 Rare Earth Pyrochlore Crystal	3
1.2 The Crystal Electric Field	4
1.3 Frustrated Systems	6
1.4 Thesis Outline	8
2 Exchange and Zeeman interactions in the RE pyrochlores	9
2.1 Spin-1/2 Systems	11

2.2	The Γ_4 Exchange Hamiltonian	12
2.3	The Γ_3 Doublet	13
2.4	The Exchange Interaction in the $\Gamma_{5,6}$ Case	13
2.5	RE Pyrochlore in Magnetic Field	15
2.5.1	The g -tensor in the Local Frame	16
2.5.2	Global Reference Frame Representation of g	16
3	Spin Wave Theory and Magnetic Ordering	18
3.1	Magnetic Order in the RE Pyrochlores	20
3.2	All In-all Out State in $\text{Nd}_2\text{Zr}_2\text{O}_7$	21
3.3	Anti-ferromagnetic Ordering in $\text{Er}_2\text{Ti}_2\text{O}_7$	23
3.4	Ferromagnetic Ordering in $\text{Yb}_2\text{Ti}_2\text{O}_7$	26
3.5	Summary	28
4	Results and discussion: Energy bands and normal mode calculations	29
4.1	Exact Analytic Diagonalization of $\mathcal{H}_{\text{ex}}^{\Gamma_{5,6}}$	31
4.1.1	Case I: $\tilde{J}_{xx} = 0$ or $J_{yy} = 0$	32
4.1.2	Case II: $\tilde{J}_{xx} = J_{yy}$	35
4.1.3	The General Case	36
4.1.4	$\text{Nd}_2\text{Zr}_2\text{O}_7$ in the [111] Magnetic Field	40
4.2	Magnon Dispersion in $\text{Er}_2\text{Ti}_2\text{O}_7$ With Antiferromagnetic ψ_2 State . . .	41
4.3	Exact Dispersions of Magnons for the Ferromagnetic State in $\text{Yb}_2\text{Ti}_2\text{O}_7$	43
4.4	Summary	51
5	Conclusions and Future Directions	52
	Bibliography	55
A	Stevens Operators and the CEF Ground States	60

B	The Local Coordinate System	62
C	The Eigenvalues and the Eigenvectors of R	64
D	Analytic Solutions of the Quartic Equation	70
E	Calculations of the BT Matrix Z	72

List of tables

1.1	High symmetry points of the FCC reciprocal lattice.	5
1.2	The values of B_p^g (in meV) for a series of rare earth titanates $R_2Ti_2O_7$ found by neutron scattering experiments [24, 30].	6
1.3	The character table of the double group D'_3 [28]. The characters are the traces of matrices representing each operation in the group. The top row lists the elements of the group divided into classes. R is a rotation by 2π , C_3 is a rotation by $2\pi/3$ and C_2 is a rotation by π . The first column lists the representations.	6
1.4	The values of the total angular momentum and the types of GSDs for different RE ions. Here Δ denotes the energy gap to the first excited state [28, 30]	7
2.1	Transformation of the pseudo-spin operators in the three ground state doublets under rotations and time reversal [28].	15
2.2	The g -tensor components for different RE pyrochlores.	16
3.1	Sets of values of the exchange parameters, the components of the g -tensor, and the rotation angle θ of $Nd_2Zr_2O_7$ obtained in four different studies [22, 23, 43, 44].	23
3.2	The values for the four exchange parameters and the components of the g -tensor for $Er_2Ti_2O_7$ [25].	25
3.3	Sets of values of the four exchange parameters of $Yb_2Ti_2O_7$ obtained in different experiments.	26

A.1 The GSD of few rare earth titanates $R_2Ti_2O_7$ [24, 30]. 61

List of figures

1.1	A schematic plot of the pyrochlore oxides unit cell showing the RE ions (red spheres), the transition metal ions (green spheres), and the rest are oxygen atoms. This picture was drawn by S. H. Curnoe.	3
1.2	The tetrahedral network of the RE ions within a cubic cell. The four tetrahedra are labeled as n , n' , n'' , and n''' . The four basis ions have been labeled with numbers 1-4. This figure was taken from [26] with permission. Copyright by the American Physical Society.	4
1.3	Example of degenerate ground states on a triangular lattice within the Ising model. On each triangle, two spins are fixed either up (blue spheres) or down (red spheres).	7
4.1	Energy bands of magnons in $\text{Nd}_2\text{Zr}_2\text{O}_7$ at zero magnetic field with exchange constants taken from Ref. [23].	33
4.2	Zero-field magnon disperions for the case when $\tilde{J}_{xx} = J_{yy} = -0.25$ and $\tilde{J}_{zz} = -0.1$. Note that these values are just mathematical and do not correspond to any RE pyrochlore material.	36
4.3	Plot of the zero-field energy dispersions of $\text{Nd}_2\text{Zr}_2\text{O}_7$. (a) Using the exchange parameters from [44] and (b) using the corresponding coupling constants from Ref. [43].	38
4.4	Plots of the exact energy dispersions at zero magnetic field for $\text{Nd}_2\text{Zr}_2\text{O}_7$ using the parameters extracted from Ref. [43]. These results show good agreement with the other findings as shown in Figure 4.5.	39

4.5	Magnon dispersions at zero magnetic field in $\text{Nd}_2\text{Zr}_2\text{O}_7$ found using the inelastic neutron scattering (background) [22] and the calculated energy dispersions (dashed curves) [43]. This picture was taken from [43] with permission. Copyright by the American Physical Society. . . .	39
4.6	Plots of the exact energy dispersions for $\text{Nd}_2\text{Zr}_2\text{O}_7$ in the [111] magnetic field using the parameters from Ref. [43] with zero canting angle. . . .	41
4.7	Plots of the neutron-scattering spectra for $\text{Nd}_2\text{Zr}_2\text{O}_7$ in the [111] magnetic field for the AIAO and the AOAI (all out-all in) states using the parameters from Ref. [43]. The red arrows at the bottom figures indicate the location of the quasi-flat bands. The whole figure was taken from [43] with permission. Copyright by the American Physical Society.	42
4.8	Plots of the zero-field energy dispersions for $\text{Er}_2\text{Ti}_2\text{O}_7$. The figure on the left is taken from previous work with permission [19]. We have considered the exchange parameters from Table 3.2. The figure on the right represents our results which matches the previous ones. Copyright by the American Physical Society.	43
4.9	Plot of the exact dispersions of magnons in $\text{Er}_2\text{Ti}_2\text{O}_7$ for magnetic field of strength $3T$ applied along $[1\bar{1}0]$ using the exchange parameters from Table 3.2. The spins are considered to be fully polarized with the applied field.	44
4.10	Neutron scattering measurements of the spin wave excitations (top row) and calculated (bottom row) dispersions of magnons in $\text{Er}_2\text{Ti}_2\text{O}_7$ for magnetic field of strength $3T$. For the first five columns, the magnetic field was taken along the $[1\bar{1}0]$ and for the rest \vec{B} is aligned with the [111] direction. The whole figure was taken from Ref. [25] with permission. Copyright by the American Physical Society.	45
4.11	Low field plots of $\varepsilon^2(\vec{k})$ for $\text{Yb}_2\text{Ti}_2\text{O}_7$ with an external magnetic field (B) applied parallel to the $[1, \bar{1}, 0]$ for different field strengths as indicated in the legends. The exchange parameters and the g -tensor were taken from Ref. [36](see Table 3.3).	45

4.12	Magnon dispersions in $\text{Yb}_2\text{Ti}_2\text{O}_7$ with an applied magnetic field of strength $2T$ along the $[1, \bar{1}, 0]$ direction. The exchange parameters and the g -tensor were taken from Ref. [36] for the sake of comparison. . . .	46
4.13	Magnon dispersions in $\text{Yb}_2\text{Ti}_2\text{O}_7$ with an applied magnetic field of strength $5T$ along the $[1, \bar{1}, 0]$ direction. The exchange parameters and the g -tensor were taken from Ref. [36] for the sake of comparison, see Table 3.3 for more details.	47
4.14	Magnon dispersions in $\text{Yb}_2\text{Ti}_2\text{O}_7$ with an applied magnetic field of strengths $5T$ (right column) and $2T$ (left column) along the $[1, \bar{1}, 0]$ direction. The exchange parameters and the g -tensor were taken from Ref. [5] (see Table 3.3) for the sake of comparison with the dispersions obtained using the parameters from Ref. [36].	48
4.15	Energy dispersions of magnons in $\text{Yb}_2\text{Ti}_2\text{O}_7$ with an applied magnetic field of strength $5T$ parallel to $[1, \bar{1}, 0]$. The white curves represent LSWA fitting over the experimental dispersions. This figure was taken from Ref. [36] with permission. Copyright by the American Physical Society.	49
4.16	Plots of the measured and calculated (calc) spin wave dispersions in $\text{Yb}_2\text{Ti}_2\text{O}_7$ for magnetic field applied along the $[1, \bar{1}, 0]$ direction. The first two rows are for the measured and the calculated dispersions at 5 T field, respectively. The lower two rows represent the experimental and computed magnon dispersions for the magnetic field with strength 2T, respectively. Note that r.l.u. stands for reciprocal lattice unit. This figure was taken from [36] with permission. Copyright by the American Physical Society.	50

List of symbols

\mathcal{H}_{CEF}	the crystal electric field Hamiltonian
B_p^q	the crystal electric field constants which vary from one material to another
O_p^q	Stevens operator which is a polynomial in the angular momentum operators $\{J_{\pm}, J_z\}$
O_h	the octahedral point group of the rare-earth pyrochlores
D_{3d}	point group the crystal electric field
D_3'	the double group for the crystal electric field
C_2	180 degree rotation around the z -axis
C_3	120 degree rotation around the z -axis
$\Gamma_{3,4,\{5,6\}}$	three different types of crystal electric field doublets that have different symmetries
\vec{S}_i	the spin operator of the rare-earth ion at the i^{th} site
\vec{B}	external magnetic field applied on the rare-earth pyrochlore crystal
g	the g -tensor which has two components $\{g_{\perp}, g_{\parallel}\}$
\mathcal{H}_{ex}	the exchange Hamiltonian between the interacting spins
\mathcal{J}_{ij}	3×3 exchange matrix
\hbar	reduced Planck's constant
$\epsilon_{\alpha\beta\gamma}$	Levi-Civita Symbol
\mathcal{H}_Z	Zeeman Hamiltonian
$M(k)$	dynamical 8×8 matrix that describes the quadratic bosonic Hamiltonian for magnons
a_i	annihilation operator of magnons at the i^{th} site
a_i^{\dagger}	creation operator of magnons at the i^{th} site
N	number of magnetic ions in the crystal
$Z(k)$	Bogoliubov transformation matrix
$\epsilon(k)$	energy dispersion of magnons
δ_{ij}	Kronecker delta which equals to 1 when $i = j$, otherwise it is zero
$\mathbb{1}$	the identity matrix

List of abbreviations

CEF	Crystal Electric Field
RE	Rare Earth
QREPs	Quantum Rare Earth Pyrochlores
NN	Nearest Neighbor
GSD	Ground State Doublet
SL	Spin Liquid
QSL	Quantum Spin Liquid
SI	Spin Ice
QSI	Quantum Spin Ice
FM	Ferromagnetic
AFM	Anti-Ferromagnetic
AIAO	All In-All Out
2I2O	two in-two out
HP	Holstein-Primakoff
MMF	Magnetic Moment Fragmentation
FCC	Face Centered Cubic
$\mathcal{R}e[x]$	Real part of x
$\mathcal{I}m[x]$	Imaginary part of x
PC	Palmer-Chalker
SWs	Spin Waves
LSWA	Linear Spin Wave Approximation
LSWT	Linear Spin Wave Theory

Chapter 1

Introduction

Rare earth (RE) pyrochlore oxides are compounds with chemical formula $A_2B_2O_7$, where A^{+3} is a rare earth ion which can be any choice of the total of 17 well-known ions such as neodymium (Nd), erbium (Er), and ytterbium (Yb), while B^{+4} is a transition metal which can be titanium (Ti), tin (Sn), zirconium (Zr), etc. A wide range of physical phenomena are observed in these compounds within the low temperature regime. For instance, the quantum spin liquid (QSL) state where the spins at the RE sites avoid any type of long-range magnetic ordering due to quantum spin fluctuations. A candidate of a RE compound that has a QSL state is $Tb_2Ti_2O_7$ [1, 2, 3], which shows no type of ordering even at low temperature [4]. Generally, quantum spin liquids are materials which do not order even at very low temperatures. Another QSL candidate is $Yb_2Ti_2O_7$ due to the existence of strong quantum fluctuations as reported in different experiments [5].

Another ordered state realized in some pyrochlores is spin ice (SI), which is a state of matter in which the magnetic moments of the RE ions follow the “ice rule” for which two spins pointing into and two out of each tetrahedron [6]. In SI systems, disorder exists even at temperatures approaching absolute zero, which is reflected in the non-zero residual entropy in those materials which is similar to the entropy of water ice [6]. The discovery of spin ice materials happened almost forty years after it was postulated by Anderson [7], and found first in $Ho_2Ti_2O_7$ [8, 9] and $Dy_2Ti_2O_7$ [10, 11]. Also, specific heat measurements reported the existence of a state called Kagome spin ice in $Dy_2Ti_2O_7$ with residual entropy for an applied magnetic field along the [111] direction [12, 13]. An important feature of SI materials is that they were the first

to support the existence of magnetic monopoles as quasi-particle excitations arising from violating the ice rule in these materials [6, 14].

Magnetic ordering happens in some of the RE pyrochlores with ferromagnetic (FM) ordering as is the case in $\text{Yb}_2\text{Ti}_2\text{O}_7$ [5, 15, 16], or anti-ferromagnetic (AFM) ordering due to quantum order by disorder in $\text{Er}_2\text{Ti}_2\text{O}_7$ [17, 18, 19]. Very recently, Han Yan *et al.* [20] have developed a theory that describes magnetic ordering in three compounds, $\text{Er}_2\text{Ti}_2\text{O}_7$, $\text{Er}_2\text{Sn}_2\text{O}_7$, and $\text{Yb}_2\text{Ti}_2\text{O}_7$. According to their findings, the magnetic ordering in $\text{Er}_2\text{Ti}_2\text{O}_7$ and $\text{Yb}_2\text{Ti}_2\text{O}_7$ plus the lack of ordering in $\text{Er}_2\text{Sn}_2\text{O}_7$ can be explained by the competition between different magnetic phases which are a FM phase, a noncolinear FM phase (ψ_4), known as Palmer-Chalker (PC) phase, and coplanar and noncoplanar AFM phases (ψ_3 and ψ_2). These materials are understood as being at the boundary between different competing magnetic phases, which altogether explains the appearance of a FM phase in $\text{Yb}_2\text{Ti}_2\text{O}_7$, AFM ordering in $\text{Er}_2\text{Ti}_2\text{O}_7$, and suppression of the magnetic ordering in $\text{Er}_2\text{Sn}_2\text{O}_7$.

Spin waves exist in materials with spin exchange interactions where the energy of those waves is quantized and the quantum of energy is called a magnon [21]. Fluctuations around the ground state can be associated with the appearance of magnons as reported in SI systems. In SI compounds, fluctuations are reflected in the appearance of different ordering such as “three in-one out” that coexists together with the overall spin ice ordering, i.e. the “two in-two out” (2I2O) state [10, 11].

Magnetic moment fragmentation (MMF) occurs in some of the rare earth pyrochlore compounds (generally in SI) [14]. In this scenario, the magnetic moment at each site is fragmented into two parts in which one is responsible for the appearance of a spin liquid phase and the other is an ordered phase. Classically, this fragmentation is due to Helmholtz decomposition of the magnetization field \vec{M} as $\vec{M} = \vec{\nabla}\Psi + \vec{\nabla} \times \vec{A}$ in which the first term is “divergence full” and the second term is “divergence free”. A very well known example of a RE oxide that shows this phenomenon is $\text{Nd}_2\text{Zr}_2\text{O}_7$ as shown experimentally in [22], and a quantum picture of the MMF in this material was given in [23]. Very recently, a neutron scattering experiment on a single crystal of $\text{Sm}_2\text{Ti}_2\text{O}_7$ shows that it also supports the MMF picture [24]. Consequently, RE pyrochlore oxides are of interest to both experimentalists and theoreticians for a better understanding of the unifying theories that govern these materials.

In this thesis, we aim to calculate the energy dispersion of magnons analytically

and numerically. We will perform calculations for different magnetically ordered states such as the “all-in-all-out” (AIAO) state in $\text{Nd}_2\text{Zr}_2\text{O}_7$, FM ordering in $\text{Yb}_2\text{Ti}_2\text{O}_7$, and AFM ordering in $\text{Er}_2\text{Ti}_2\text{O}_7$. These systems have been studied before with the energy dispersions have been found numerically for each case [5, 22, 25]. In this work we pay more attention to the analytic calculations of the energy dispersions and, whenever possible, the normal modes as well. We have also reproduced the numerical results for comparison.

1.1 Rare Earth Pyrochlore Crystal

The actual lattice of the pyrochlore crystal is very complicated, as shown in Figure 1.1. The chemical formula of the RE pyrochlore is $A_2B_2O_7$, where each of the rare earth ions (A) and the transition metal (B) form a corner-sharing tetrahedral network. RE pyrochlores belong to the space group $Fd\bar{3}m$ which has a FCC lattice with the RE ions located on the 16d Wyckoff positions.

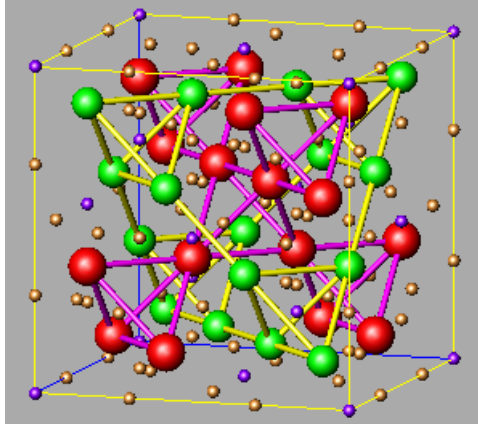


Figure 1.1: A schematic plot of the pyrochlore oxides unit cell showing the RE ions (red spheres), the transition metal ions (green spheres), and the rest are oxygen atoms. This picture was drawn by S. H. Curnoe.

Considering only the rare earth ions, the primitive unit cell is a single tetrahedron with four basis ions residing on the positions $a(5/8, 5/8, 5/8)$, $a(3/8, 3/8, 5/8)$, $a(3/8, 5/8, 3/8)$, and $a(5/8, 3/8, 3/8)$ which are numbered from 1 to 4, respectively, where a is the length of the cubic cell. One can map the whole rare earth lattice by using the FCC lattice translations which are $\vec{u}_1 = \frac{a}{2}(1, 1, 0)$, $\vec{u}_2 = \frac{a}{2}(1, 0, 1)$, and

$\vec{u}_3 = \frac{a}{2}(0, 1, 1)$, forming a corner-sharing tetrahedral network of those ions. In Figure 1.2, we show a schematic diagram of the RE lattice.

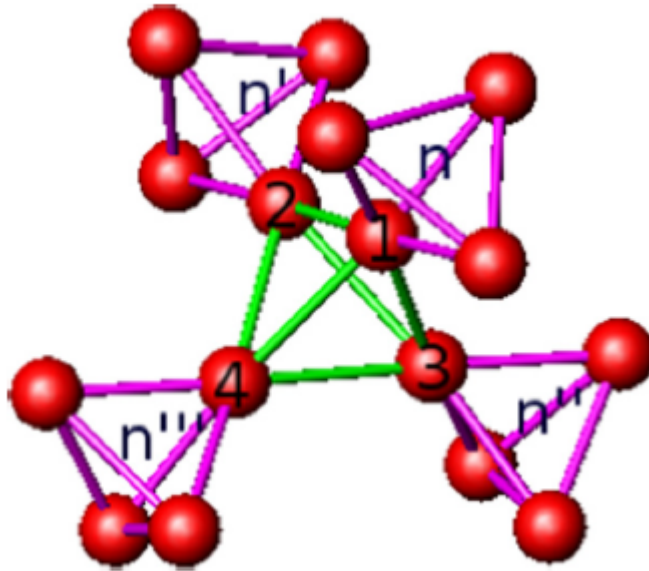


Figure 1.2: The tetrahedral network of the RE ions within a cubic cell. The four tetrahedra are labeled as n , n' , n'' , and n''' . The four basis ions have been labeled with numbers 1-4. This figure was taken from [26] with permission. Copyright by the American Physical Society.

We are also interested in the reciprocal space of the FCC lattice and its symmetry points. The positions of the high symmetry points in k -space are given in Table 1.1.

1.2 The Crystal Electric Field

The treatment of all the RE pyrochlores is based on the nearly free magnetic ion model in which the effect of the other ions in the lattice is included in the crystal electric field (CEF). The free space isotropy is destroyed in the presence of the CEF which results in reducing the dimensionality to that of the irreducible representation of the associated point group D_{3d} , the symmetry of the CEF at the RE site. Consequently, the degeneracies are lifted [27]. In our case, if the RE ion A^{+3} has a total angular momentum J , the $2J+1$ fold degeneracy will split into singlets and doublets due to the

Table 1.1: High symmetry points of the FCC reciprocal lattice.

Symmetry Point	Reciprocal Position
Γ	(0,0,0)
X	$\frac{2\pi}{a}(0,1,0)$
W	$\frac{\pi}{a}(1,2,0)$
L	$\frac{\pi}{a}(1,1,1)$
K	$\frac{3\pi}{2a}(1,1,0)$
U	$\frac{\pi}{2a}(1,4,1)$

CEF [28]. Generally, the ground state for most of the quantum rare-earth pyrochlores (QREPs) is a doublet except for Thulium (Tm) which has a singlet ground state [29, 30]. Classically, the CEF Hamiltonian is a Coulomb potential $V(x, y, z)$ with D_{3d} symmetry. The next step is to do Taylor expansion of the potential $V(x, y, z)$ where only certain terms will appear in the expansion due to symmetry. It was shown that only the first six terms in the series are relevant and the inclusion of higher order terms will not provide new physics to the problem [27, 30], i.e. higher order terms are very small. To quantize the CEF Hamiltonian, we use Wigner-Eckart theorem that allows the replacement of the position operators $\{x, y, z\}$ with the angular momentum operators $\{J_x, J_y, J_z\}$ giving the following CEF Hamiltonian [30]

$$\mathcal{H}_{\text{CEF}} = B_2^0 \mathcal{O}_2^0 + B_4^0 \mathcal{O}_4^0 + B_4^3 \mathcal{O}_4^3 + B_6^0 \mathcal{O}_6^0 + B_6^3 \mathcal{O}_6^3 + B_6^6 \mathcal{O}_6^6, \quad (1.1)$$

where B_p^q are constant parameters that vary for different materials, and \mathcal{O}_p^q are Stevens operators which are polynomials in $\{J_z, J_{\pm}\}$ with degree p , with q being the power of J_{\pm} , i.e. \mathcal{O}_p^0 is a polynomial of degree p in J_z [33]. The explicit forms of the six Stevens operators \mathcal{O}_p^q are listed in Appendix A. The determination of the parameters B_p^q have been done by different groups using neutron scattering experiments and experimental data fitting [30]. In the Table 1.2 below, we list the given values of the parameters B_p^q for several of RE titanate pyrochlores [24, 30].

Thus, using the values of the CEF parameters given in the Table 1.2 together with Stevens operators given in Appendix A, one can easily find the CEF energies for each of the RE titanates by expressing the CEF Hamiltonian in certain basis which is usually taken to be the $|m_J\rangle$, where $m_J = -J, -J + 1, \dots, J - 1, J$, then diagonalizing \mathcal{H}_{CEF} will give the energies of the singlet and the doublet states. The eigenstates of \mathcal{H}_{CEF} belong to different irreducible representation of the point group D_3' as given in

Table 1.2: The values of B_p^q (in meV) for a series of rare earth titanates $R_2Ti_2O_7$ found by neutron scattering experiments [24, 30].

R	B_2^0	B_4^0	B_4^3	B_6^0	B_6^3	B_6^6
Tb	-0.34	4.9×10^{-3}	4.3×10^{-2}	-7.9×10^{-6}	1.3×10^{-4}	-1.08×10^{-4}
Dy	-0.20	-2.2×10^{-3}	-1.9×10^{-2}	6.6×10^{-6}	-1.09×10^{-4}	9.0×10^{-5}
Ho	-6.8×10^{-2}	-1.13×10^3	-1.01×10^{-2}	-7.4×10^{-6}	1.23×10^{-4}	-1.01×10^{-4}
Er	7.5×10^{-2}	1.41×10^{-3}	1.25×10^{-2}	1.09×10^{-5}	-1.8×10^{-4}	1.5×10^{-4}
Yb	0.87	-4.2×10^{-2}	-0.43	6.6×10^{-4}	-1.09×10^{-2}	8.9×10^{-3}
Sm	3.397	0.123	8.28×10^{-8}	—	—	—

Table 1.3. For integral J , the eigenstates of the CEF Hamiltonian belong to three different representations which are two singlets Γ_1 and Γ_2 and a non-Kramers doublet Γ_3 . On the other hand, for half-integral J there are two types of Kramer doublets denoted by Γ_4 and $\Gamma_{5,6}$. Considering the CEF ground state doublets (GSD), we are interested in cases for which the separation between this doublet and the first excited state is of the order 100 K [28]. These systems are therefore considered as effective spin-1/2 systems, i.e. quantum systems. We have tabulated the energy gap to the first excited state for different rare-earth ions in Table 1.4.

Table 1.3: The character table of the double group D_3' [28]. The characters are the traces of matrices representing each operation in the group. The top row lists the elements of the group divided into classes. R is a rotation by 2π , C_3 is a rotation by $2\pi/3$ and C_2 is a rotation by π . The first column lists the representations.

D_3'	E	R	$2C_3$	$2RC_3$	$3C_2$	$3RC_2$
Γ_1	1	1	1	1	1	1
Γ_2	1	1	1	1	-1	-1
Γ_3	2	2	-1	-1	0	0
Γ_4	2	-2	1	-1	0	0
$\Gamma_{5,6}$	1	-1	-1	1	i	$-i$
	1	-1	-1	1	$-i$	i

1.3 Frustrated Systems

A spin system is frustrated when there is no configuration which simultaneously minimizes the interaction energy between all pairs of spins. This typically leads to degenerate ground states. The isotropic Heisenberg interaction between spins is governed

Table 1.4: The values of the total angular momentum and the types of GSDs for different RE ions. Here Δ denotes the energy gap to the first excited state [28, 30]

RE ion	J	GSD	$\Delta(\text{meV})$	Representation
Tb	6	Γ_3	1.50	Γ_3
Dy	$\frac{15}{2}$	$\Gamma_{5,6}$	30.9	$\Gamma_{5,6}$
Ho	8	Γ_3	20.7	Γ_3
Er	$\frac{15}{2}$	Γ_4	6.30	Γ_4
Yb	$\frac{7}{2}$	Γ_4	53.4	Γ_4

by the Hamiltonian

$$\mathcal{H} = J \sum_{\langle ij \rangle} \vec{S}_i \cdot \vec{S}_j. \quad (1.2)$$

with $J < 0$ for ferromagnetic systems, and $J > 0$ for anti-ferromagnetic spin exchange. The simplest frustrated system is the triangular lattice where at each triangle there are different choices of the spin orientations that minimize the energy of \mathcal{H} for the AFM interaction. For illustration, Figure 1.3 below shows two different spin orientations on the equilateral triangle each with the same energy $E_{\text{tri}} = -2JS^2$. The total number of possible configurations that give the same minimum energy is 6.

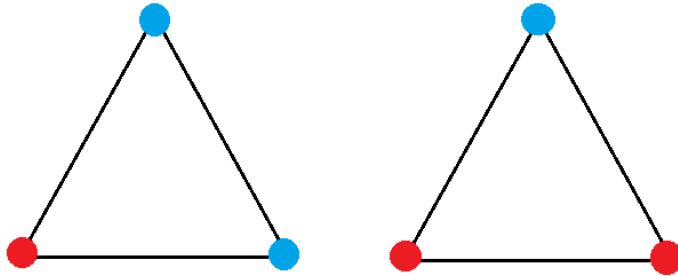


Figure 1.3: Example of degenerate ground states on a triangular lattice within the Ising model. On each triangle, two spins are fixed either up (blue spheres) or down (red spheres).

Going to three dimensions, the pyrochlore lattice is a good example of a highly frustrated system on which there are more possible configurations that give rise to the same lowest energy and thus are considered as highly degenerate systems. Consequently, these systems accommodate various low temperature magnetic states.

1.4 Thesis Outline

The flow of the work goes as follows. In Chapter 2, we introduce the nearest-neighbor exchange interaction and come across the exchange Hamiltonian for each type of the ground state doublets, then we discuss interactions with magnetic fields through the inclusion of the Zeeman Hamiltonian which will be represented in local and global coordinates. Secondly, in Chapter 3, we discuss spin waves and how to construct the magnon Hamiltonian for the three doublets using the Holstein-Primakoff transformation, and we end the chapter with three examples of RE pyrochlore each of which the quadratic magnonic Hamiltonian was constructed. Furthermore, we discuss the diagonalization of the magnon Hamiltonian in Chapter 4, and then present our analytic results for three RE pyrochlore materials which are $\text{Nd}_2\text{Zr}_2\text{O}_7$, $\text{Er}_2\text{Ti}_2\text{O}_7$, and $\text{Yb}_2\text{Ti}_2\text{O}_7$ in their ordered states and in the presence of an external magnetic field. Finally, we conclude our work in Chapter 5.

Chapter 2

Exchange and Zeeman interactions in the RE pyrochlores

The spin-spin interactions between magnetic ions on the pyrochlore lattice, to a good approximation, are written in bilinear terms of the individual spins as [28]

$$\mathcal{H}_S = \sum_{\langle ij \rangle} \vec{S}_i^T J_{ij} \vec{S}_j + \frac{1}{2} D a^3 \sum_{ij} \left[\frac{\vec{S}_i \cdot \vec{S}_j}{|\vec{R}_{ij}|^3} - 3 \frac{(\vec{S}_i \cdot \vec{R}_{ij})(\vec{S}_j \cdot \vec{R}_{ij})}{|\vec{R}_{ij}|^5} \right], \quad (2.1)$$

where $\langle ij \rangle$ denotes that the sum is over the nearest neighbour sites $\{i, j\}$, $\vec{S}_j = (S_{jx}, S_{jy}, S_{jz})$, J_{ij} is a 3×3 matrix containing the short-range exchange parameters, D is the strength of the dipole-dipole term (the second term above) to be included in the case of long-range interactions, a is the nearest neighbour (NN) distance (or the edge length of the tetrahedron), and \vec{R}_{ij} is the distance vector between the interacting spins. In this work, we limit ourselves to the NN interactions which results in the Hamiltonian

$$\mathcal{H}_S = \sum_{\langle ij \rangle} \vec{S}_i^T \mathcal{J}_{ij} \vec{S}_j. \quad (2.2)$$

where the NN contribution of the second term of Eq. (2.1) has been absorbed in the effective exchange parameters matrix \mathcal{J}_{ij} in Eq. (2.2) above. The NN exchange Hamiltonian for the rare earth ions in the pyrochlore lattice takes the following general form [28]

$$\mathcal{H}_{\text{ex}} = \sum_{i=1}^4 \mathcal{J}_i X_i, \quad (2.3)$$

where $\{\mathcal{J}_i\}_{i=1}^4$ are the exchange parameters, and the four independent terms $\{X_i\}$ are [28]

$$X_1 = -\frac{1}{3} \sum_{\langle ij \rangle} S_{iz} S_{jz}, \quad (2.4)$$

$$X_2 = -\frac{\sqrt{2}}{3} \sum_{\langle ij \rangle} [\Lambda_{ij}(S_{iz} S_{j+} + S_{jz} S_{i+}) + \Lambda_{ij}^*(S_{iz} S_{j-} + S_{jz} S_{i-})], \quad (2.5)$$

$$X_3 = \frac{1}{3} \sum_{\langle ij \rangle} [\Lambda_{ij}^* S_{i+} S_{j+} + \Lambda_{ij} S_{i-} S_{j-}], \quad (2.6)$$

$$X_4 = -\frac{1}{6} \sum_{\langle ij \rangle} (S_{i+} S_{j-} + S_{i-} S_{j+}), \quad (2.7)$$

where $S_{j\pm} = S_{jx} \pm iS_{jy}$ and

$$\Lambda = \begin{pmatrix} 0 & 1 & \epsilon & \epsilon^* \\ 1 & 0 & \epsilon^* & \epsilon \\ \epsilon & \epsilon^* & 0 & 1 \\ \epsilon^* & \epsilon & 1 & 0 \end{pmatrix}, \quad (2.8)$$

with $\epsilon = \exp(i2\pi/3)$. Aside from being independent terms, each of the $\{X_i\}$ terms above is invariant under group rotations and time reversal and their sum is isotropic, i.e. $\sum_{i=1}^4 X_i = \sum_{\langle ij \rangle} \vec{S}_i \cdot \vec{S}_j$ [28]. In the above expressions the local coordinate system (see Appendix B) has been used. We now express this Hamiltonian in a form which will be useful in our discussions later [28],

$$\mathcal{H}_{\text{ex}} = \sum_{\langle ij \rangle} \mathcal{H}_{ij}, \quad (2.9)$$

where

$$\begin{aligned} \mathcal{H}_{ij} = & J_{zz} S_{iz} S_{jz} - J_{\pm} (S_{i+} S_{j-} + S_{i-} S_{j+}) + J_{\pm\pm} (\Lambda_{ij}^* S_{i+} S_{j+} + \Lambda_{ij} S_{i-} S_{j-}) \\ & - J_{z\pm} [\Lambda_{ij} (S_{iz} S_{j+} + S_{jz} S_{i+}) + \Lambda_{ij}^* (S_{iz} S_{j-} + S_{jz} S_{i-})], \end{aligned} \quad (2.10)$$

with $\{J_{zz}, J_{\pm}, J_{\pm\pm}, J_{z\pm}\}$ being the renormalized exchange parameters. Note that Eq. (2.9) is equivalent to Eq. (2.2), with the exchange matrix \mathcal{J}_{ij} in the form

$$\mathcal{J}_{ij} = 2 \begin{pmatrix} -J_{\pm} + \mathcal{U}_{ij}J_{\pm\pm} & \mathcal{V}_{ij}J_{\pm\pm} & -\mathcal{U}_{ij}J_{z\pm} \\ \mathcal{V}_{ij}J_{\pm\pm} & -J_{\pm} - \mathcal{U}_{ij}J_{\pm\pm} & \mathcal{V}_{ij}J_{z\pm} \\ -\mathcal{U}_{ij}J_{z\pm} & \mathcal{V}_{ij}J_{z\pm} & J_{zz}/2 \end{pmatrix}, \quad (2.11)$$

where

$$\mathcal{U}_{ij} = \text{Re}[\Lambda_{ij}], \mathcal{V}_{ij} = \text{Im}[\Lambda_{ij}]. \quad (2.12)$$

Thus, we have discussed the most general NN exchange Hamiltonian which will be used to study different rare-earth pyrochlore systems with an effective crystal electric field ground state doublet. In the next sections, we will review the properties of spin-1/2 systems and we will discuss three classes of RE pyrochlores with their properties and the exchange Hamiltonian in each case. At the end, we will come across the Zeeman interaction in each of these class of materials.

2.1 Spin-1/2 Systems

Spin operators are one of the most important observables in quantum mechanics especially when it comes to describing magnetic interactions and ions in magnetic fields, for example in the Zeeman interaction. These operators satisfy special commutation relations,

$$[S_j^\alpha, S_l^\beta] = i\hbar\epsilon_{\alpha\beta\gamma}\delta_{jl}S_j^\gamma, \quad (2.13)$$

where S_j^α denotes the α -component of the spin operator at the j^{th} site, δ_{jl} is the Kronecker delta function, and $\epsilon_{\alpha\beta\gamma}$ is the Levi-Civita symbol [34]. We generally represent the spins in the $|\{s_i\}, \{m_i\}\rangle$ basis (generally known as Zeeman basis), where s_i is the total spin of the ion at the i^{th} , $m_i = -s_i, -s_i + 1, \dots, s_i - 1, s_i$ is the spin quantum number. Thus, the eigenvalue equations are

$$S_j^2|\{s_i\}, \{m_i\}\rangle = \hbar^2 s_j(s_{j+1} + 1)|\{s_i\}, \{m_i\}\rangle, \quad (2.14)$$

$$S_{jz}|\{s_i\}, \{m_i\}\rangle = \hbar m_j|\{s_i\}, \{m_i\}\rangle, \quad (2.15)$$

where $S_j^2 = S_{jx}^2 + S_{jy}^2 + S_{jz}^2$. We define the raising (+) and the lowering (-) operators as follows

$$S_{j\pm} = S_{jx} \pm iS_{jy}. \quad (2.16)$$

Note that $|\{s_i\}, \{m_i\}\rangle$ is not an eigenvector of $S_{j\pm}$, instead the action of these operators on the basis ket is given below [34]

$$S_{j\pm}|\{s_i\}, \{m_i\}\rangle = \hbar\sqrt{s_j(s_j+1) - m_j(m_j\pm 1)}|\{s_i\}, \{m_1, \dots, m_j\pm 1, \dots, m_N\}\rangle. \quad (2.17)$$

We will now consider the interesting two-states system with $s = \frac{1}{2}$. The basis states for this system are denoted by $|\pm\rangle = |\frac{1}{2}, \pm\frac{1}{2}\rangle$. Moreover, the spin components are represented in a matrix form in the above basis as

$$S_{i\alpha} = \frac{\hbar}{2}\sigma_{i\alpha}, \quad (2.18)$$

where $\alpha = x, y, z$, and $\sigma_{i\alpha}$ are Pauli matrices which are given below

$$\sigma_{ix} = \begin{pmatrix} 0 & 1 \\ 1 & 0 \end{pmatrix}, \quad \sigma_{iy} = \begin{pmatrix} 0 & -i \\ i & 0 \end{pmatrix}, \quad \sigma_{iz} = \begin{pmatrix} 1 & 0 \\ 0 & -1 \end{pmatrix}. \quad (2.19)$$

In addition to the matrix representation of the spin, we would like to mention the following expression of $S_{i\alpha}$ in terms of the basis kets and bras:

$$S_{ix} = |+\rangle\langle-| + |-\rangle\langle+|, \quad S_{iy} = -i|+\rangle\langle-| + i|-\rangle\langle+|, \quad S_{iz} = |+\rangle\langle+| - |-\rangle\langle-|. \quad (2.20)$$

We can define the pseudo-spin operators of the same form for the three classes of doublets using the ground state doublet (GSD) wavefunctions given in Table A.1, where we generally use the replacement $|\pm\rangle \rightarrow |\psi_0^\pm\rangle$ in Eq. (2.20), where $|\psi_0^\pm\rangle$ is the GSD wavefunction.

2.2 The Γ_4 Exchange Hamiltonian

As we have discussed in Section 2.1, the pseudo-spin operators are defined in terms of the GSD given in Table A.1, which is analogous to Eq. (2.20). In this class, the Γ_4 doublet, the pseudo-spin operators are exact spinors, i.e. they transform like as

the real spin- $\frac{1}{2}$ operators. Under C_3 rotations about the local z -axis, the operator S_{iz} remains unaffected while the operator $S_{i\pm}$ picks a phase of $e^{\pm\frac{2\pi i}{3}}$. On the other hand, under the C_2 rotation about the local x -axis, the z -component of the spin operator changes sign while S_{i+} transforms to S_{i-} and vice versa. Finally, the spin components all change sign under time reversal. Thus, the exchange Hamiltonian suitable for this class is the one given in Eq. (2.9) with $s_i = \frac{1}{2}$ and the exchange constants are renormalized by the numbers $j = 2\langle\psi_0^+|S_z|\psi_0^+\rangle$ and $t = \langle\psi_0^+|S_+|\psi_0^-\rangle$ [28]. Examples of quantum rare-earth pyrochlore (QREP) that belong to this class are $\text{Yb}_2\text{Ti}_2\text{O}_7$, $\text{Yb}_2\text{Sn}_2\text{O}_7$, $\text{Er}_2\text{Ti}_2\text{O}_7$, and $\text{Er}_2\text{Sn}_2\text{O}_7$. One can easily use the data provided in Table A.1 together with Eq. (2.20) to verify the properties of the spin operators associated with this category which requires the knowledge of how the basis kets $|\{s_i\}, \{m_i\}\rangle$ transform under time reversal and space rotations [35].

2.3 The Γ_3 Doublet

In the Γ_3 class of doublets, which are non-Kramer's doublets as they are associated with integral spins, the spin operators obtained by Eq. (2.20) under C_2 and C_3 rotations transform exactly the same way as the Γ_4 operators. However, under time reversal, the operators $S_{i\pm}$ don't change sign. Thus, to keep the Hamiltonian unchanged under time reversal, the $J_{z\pm}$ term must vanish, giving the following general exchange Hamiltonian for this system,

$$\mathcal{H}_{\text{ex}} = \sum_{\langle ij \rangle} [J_{zz}S_{iz}S_{jz} - J_{\pm}(S_{i+}S_{j-} + S_{i-}S_{j+}) + J_{\pm\pm}(\Lambda_{ij}^*S_{i+}S_{j+} + \Lambda_{ij}S_{i-}S_{j-})]. \quad (2.21)$$

Examples of QREP that belong to this class are $\text{Ho}_2\text{Ti}_2\text{O}_7$ and $\text{Pr}_2\text{Sn}_2\text{O}_7$ [28].

2.4 The Exchange Interaction in the $\Gamma_{5,6}$ Case

The symmetry properties of the $\Gamma_{5,6}$ type of doublets are similar to those in the Γ_4 class except that under C_3 operations the operators in this doublet remain unchanged. Consequently, the phases Λ_{ij} are unity and thus Eq. (2.10) becomes

$$\mathcal{H}_{ij} = J_{zz}S_{iz}S_{jz} - J_{\pm}(S_{i+}S_{j-} + S_{i-}S_{j+}) + J_{\pm\pm}(S_{i+}S_{j+} + S_{i-}S_{j-})$$

$$- J_{z\pm} [S_{iz}S_{j+} + S_{jz}S_{i+} + S_{iz}S_{j-} + S_{jz}S_{i-}]. \quad (2.22)$$

By simplifying terms, the total anisotropic exchange Hamiltonian for this type of doublet is

$$\mathcal{H}_{\text{ex}} = \sum_{\langle ij \rangle} [J_{zz}S_{iz}S_{jz} + J_{yy}S_{iy}S_{jy} + J_{xx}S_{ix}S_{jx} + J_{zx}(S_{iz}S_{jx} + S_{ix}S_{jz})]. \quad (2.23)$$

We can do a “global” rotation in the xz -plane such that the fourth term in Eq. (2.23) is eliminated. This transformation reads

$$S_{ix} = \cos \theta \tilde{S}_{ix} - \sin \theta \tilde{S}_{iz}, \quad S_{iz} = \sin \theta \tilde{S}_{ix} + \cos \theta \tilde{S}_{iz}, \quad (2.24)$$

where $\tilde{S}_{i\alpha}$ is the corresponding spin component in the rotated frame, and we choose θ to satisfy

$$\tan(2\theta) = \frac{J_{zx}}{J_{xx} - J_{zz}}. \quad (2.25)$$

Thus, the exchange Hamiltonian in this case becomes

$$\mathcal{H}_{\text{ex}} = \sum_{\langle ij \rangle} [\tilde{J}_{zz}\tilde{S}_{iz}\tilde{S}_{jz} + J_{yy}S_{iy}S_{jy} + \tilde{J}_{xx}\tilde{S}_{ix}\tilde{S}_{jx}], \quad (2.26)$$

where

$$\tilde{J}_{xx} = \frac{J_{xx} + J_{zz} + \sqrt{(J_{xx} - J_{zz})^2 + J_{zx}^2}}{2}, \quad \tilde{J}_{zz} = \frac{J_{xx} + J_{zz} - \sqrt{(J_{xx} - J_{zz})^2 + J_{zx}^2}}{2}. \quad (2.27)$$

Examples of rare earth pyrochlores with this class of doublet include $\text{Nd}_2\text{Zr}_2\text{O}_7$ which is the first among the RE pyrochlores that verifies the MMF picture classically and quantum mechanically [22, 23]. Other RE pyrochlores in this category are $\text{Nd}_2\text{Ir}_2\text{O}_7$, $\text{Dy}_2\text{Ti}_2\text{O}_7$, and $\text{Sm}_2\text{Ti}_2\text{O}_7$ [24, 28].

To summarize the previous three sections, we present the properties of the pseudo-spin operators in the three cases under different symmetry operations as given in Table 2.1. In the next section, we will discuss the effect of magnetic field on the rare earth ions by including the Zeeman term in the total Hamiltonian as this is needed for some systems in which magnons are excited in the presence of an external magnetic field such as the case in $\text{Yb}_2\text{Ti}_2\text{O}_7$.

Table 2.1: Transformation of the pseudo-spin operators in the three ground state doublets under rotations and time reversal [28].

GSD	C_2	C_3	TimeReversal
Γ_3	$S_z \rightarrow -S_z, S_{\pm} \rightarrow S_{\mp}$	$S_z \rightarrow S_z, S_{\pm} \rightarrow \epsilon^{\pm 1} S_{\pm}$	$S_z \rightarrow -S_z, S_{\pm} \rightarrow S_{\mp}$
Γ_4	$S_z \rightarrow -S_z, S_{\pm} \rightarrow S_{\mp}$	$S_z \rightarrow S_z, S_{\pm} \rightarrow \epsilon^{\pm 1} S_{\pm}$	$S_z \rightarrow -S_z, S_{\pm} \rightarrow -S_{\pm}$
$\Gamma_{5,6}$	$S_z \rightarrow -S_z, S_{\pm} \rightarrow S_{\mp}$	$S_z \rightarrow S_z, S_{\pm} \rightarrow S_{\pm}$	$S_z \rightarrow -S_z, S_{\pm} \rightarrow -S_{\pm}$

2.5 RE Pyrochlore in Magnetic Field

Classically, a particle with magnetic moment $\vec{\mu}_i$ when placed in external magnetic field \vec{B} , it will experience a torque $\vec{\tau}_i = \vec{\mu}_i \times \vec{B}$ which causes the moment to align with the applied field. The total energy of a system of magnetic moments in magnetic field is

$$E = - \sum_i \vec{\mu}_i \cdot \vec{B}. \quad (2.28)$$

The quantum version of this energy for a system of particles with spins $\{\vec{S}_i\}$ is

$$\mathcal{H}_Z = -\gamma \sum_i \vec{B} \cdot \vec{S}_i, \quad (2.29)$$

where γ is the gyromagnetic ratio [34]. \mathcal{H}_Z is the Zeeman Hamiltonian, which generally written in the form

$$\mathcal{H}_Z = \mu_B \sum_i \sum_{\alpha, \beta=x,y,z} B_{i\alpha} g_{\alpha, \beta} S_{i\beta} = - \sum_i \vec{B} \cdot \vec{\mu}_i, \quad (2.30)$$

where μ_B is the Bohr magneton, and the g -tensor is a 3×3 matrix which is a generalized version of the gyromagnetic ratio γ mentioned above. Thus, the effective Hamiltonian for QREP systems is

$$\mathcal{H} = \mathcal{H}_{\text{ex}} + \mathcal{H}_Z, \quad (2.31)$$

where \mathcal{H}_{ex} is given in Eq. (2.9). In the following sections, we will discuss the expressions of the g -tensor in the local and the global reference frames, and we will also provide numerical values of its components for different QREPs.

2.5.1 The g -tensor in the Local Frame

In the local frame discussed in Appendix B, the g -tensor has only two components denoted by g_{\parallel} and g_{\perp}

$$g = \begin{pmatrix} g_{\perp} & 0 & 0 \\ 0 & g_{\perp} & 0 \\ 0 & 0 & g_{\parallel} \end{pmatrix}. \quad (2.32)$$

Thus, the Zeeman contribution to the total Hamiltonian is

$$\mathcal{H}_Z = -\mu_B \sum_i \left[g_{\parallel} B_{iz} \hat{S}_{iz} + g_{\perp} \left(B_{ix} \hat{S}_{ix} + B_{iy} \hat{S}_{iy} \right) \right], \quad (2.33)$$

where the $\{B_{i\alpha}\}$ are the components of the applied field with respect to the local coordinate frame. Note that for Γ_3 and $\Gamma_{5,6}$ doublets, we have $g_{\perp} = 0$ because $\langle \psi_0^- | S_- | \psi_0^+ \rangle$ vanishes in those doublets [28], while for the Γ_4 case neither component of the g -tensor is zero. Note that g_{\perp} and g_{\parallel} will be normalized by $\langle \psi_0^- | S_- | \psi_0^+ \rangle$ and $\langle \psi_0^+ | S_z | \psi_0^+ \rangle$, respectively [28]. In Table 2.2, we list the components of g for several materials [5, 24, 36, 37, 38, 39].

Table 2.2: The g -tensor components for different RE pyrochlores.

REPOs	g_{\perp}	g_{\parallel}
Yb ₂ Ti ₂ O ₇ [5]	4.17	2.14
Yb ₂ Ti ₂ O ₇ [36]	4.32	1.80
Yb ₂ Ti ₂ O ₇ [37]	4.09	2.06
Yb ₂ Sn ₂ O ₇ [38]	4.20	1.10
Er ₂ Ti ₂ O ₇ [39]	5.97	2.45
Sm ₂ Ti ₂ O ₇ [24]	0	0.857

2.5.2 Global Reference Frame Representation of g

For completeness, we would like to express the g -tensor in the global references frame defined by the crystal axes. This will require the use of Eq. (2.32) together with the R_i matrices defined in Appendix B. This will result in a site-dependent g that takes the form

$$g_i = R_i g R_i^T, \quad (2.34)$$

where T stands for the transpose of the matrix. Thus, the four g -tensor matrices (for the four different sites) are

$$g_1 = \begin{pmatrix} \frac{2g_{\perp}}{3} + \frac{g_{\parallel}}{3} & \frac{g_{\parallel}}{3} - \frac{g_{\perp}}{3} & \frac{g_{\parallel}}{3} - \frac{g_{\perp}}{3} \\ \frac{g_{\parallel}}{3} - \frac{g_{\perp}}{3} & \frac{2g_{\perp}}{3} + \frac{g_{\parallel}}{3} & \frac{g_{\parallel}}{3} - \frac{g_{\perp}}{3} \\ \frac{g_{\parallel}}{3} - \frac{g_{\perp}}{3} & \frac{g_{\parallel}}{3} - \frac{g_{\perp}}{3} & \frac{2g_{\perp}}{3} + \frac{g_{\parallel}}{3} \end{pmatrix}, \quad (2.35)$$

$$g_2 = \begin{pmatrix} \frac{2g_{\perp}}{3} + \frac{g_{\parallel}}{3} & \frac{g_{\parallel}}{3} - \frac{g_{\perp}}{3} & \frac{g_{\perp}}{3} - \frac{g_{\parallel}}{3} \\ \frac{g_{\parallel}}{3} - \frac{g_{\perp}}{3} & \frac{2g_{\perp}}{3} + \frac{g_{\parallel}}{3} & \frac{g_{\perp}}{3} - \frac{g_{\parallel}}{3} \\ \frac{g_{\perp}}{3} - \frac{g_{\parallel}}{3} & \frac{g_{\perp}}{3} - \frac{g_{\parallel}}{3} & \frac{2g_{\perp}}{3} + \frac{g_{\parallel}}{3} \end{pmatrix}, \quad (2.36)$$

$$g_3 = \begin{pmatrix} \frac{2g_{\perp}}{3} + \frac{g_{\parallel}}{3} & \frac{g_{\perp}}{3} - \frac{g_{\parallel}}{3} & \frac{g_{\parallel}}{3} - \frac{g_{\perp}}{3} \\ \frac{g_{\perp}}{3} - \frac{g_{\parallel}}{3} & \frac{2g_{\perp}}{3} + \frac{g_{\parallel}}{3} & \frac{g_{\perp}}{3} - \frac{g_{\parallel}}{3} \\ \frac{g_{\parallel}}{3} - \frac{g_{\perp}}{3} & \frac{g_{\perp}}{3} - \frac{g_{\parallel}}{3} & \frac{2g_{\perp}}{3} + \frac{g_{\parallel}}{3} \end{pmatrix}, \quad (2.37)$$

$$g_4 = \begin{pmatrix} \frac{2g_{\perp}}{3} + \frac{g_{\parallel}}{3} & \frac{g_{\perp}}{3} - \frac{g_{\parallel}}{3} & \frac{g_{\perp}}{3} - \frac{g_{\parallel}}{3} \\ \frac{g_{\perp}}{3} - \frac{g_{\parallel}}{3} & \frac{2g_{\perp}}{3} + \frac{g_{\parallel}}{3} & \frac{g_{\parallel}}{3} - \frac{g_{\perp}}{3} \\ \frac{g_{\perp}}{3} - \frac{g_{\parallel}}{3} & \frac{g_{\parallel}}{3} - \frac{g_{\perp}}{3} & \frac{2g_{\perp}}{3} + \frac{g_{\parallel}}{3} \end{pmatrix}. \quad (2.38)$$

Thus, we have determined the connection between the global and the local representations of the effective Hamiltonian $\mathcal{H}_{\text{eff}} = \mathcal{H}_{\text{ex}} + \mathcal{H}_Z$. In the next chapter, we will use the local representation of the effective Hamiltonian to study magnons in different QREP systems which host different types of magnetic ordering in the low temperature regime.

Chapter 3

Spin Wave Theory and Magnetic Ordering

The low energy excitations of interacting spins are referred to as spin waves (SW) or magnons [21]. To study these magnons, we use the Holstein-Primakoff (HP) transformation which maps the spin operators to creation and annihilation bosonic operators as defined below [21, 40]

$$S_{i+} = \left(\sqrt{2s - a_i^\dagger a_i} \right) a_i, \quad S_{i-} = (S_{i+})^\dagger, \quad S_{iz} = s - a_i^\dagger a_i, \quad (3.1)$$

where s is the spin which is one-half in our case, a_i^\dagger and a_i are the creation and the annihilation operators of magnons, respectively, which satisfy the following commutators

$$[a_{ni}, a_{mj}^\dagger] = \delta_{ij} \delta_{nm} \quad \text{and} \quad [a_{ni}, a_{mj}] = [a_{ni}^\dagger, a_{mj}^\dagger] = 0, \quad (3.2)$$

where $\{i, j\}$ labels the sites of the RE ions on a tetrahedron, and $\{n, m\}$ refers to the tetrahedra that contain the magnetic ions. Note that the appearance of the operator $\sqrt{2s - a_i^\dagger a_i}$ in Eq. (3.1) makes the calculations of spin waves in the spin systems hard, which motivates us to use some sort of approximation as follows. First, we expand the operator $\sqrt{2s - a_i^\dagger a_i}$ in a Taylor series,

$$\sqrt{2s - a_i^\dagger a_i} = \sqrt{2s} \left[1 - \frac{a_i^\dagger a_i}{4s} + \dots \right]. \quad (3.3)$$

Considering only the first leading term in Eq. (3.3) is an approximation generally referred to as the linear spin wave approximation (LSWA), in which the HP transformation becomes

$$S_{i+} \approx \sqrt{2S}a_i, S_{i-} \approx \sqrt{2S}a_i^\dagger, S_{iz} = S - a_i^\dagger a_i. \quad (3.4)$$

Note that the above HP in the LSWA satisfy the following commutators (in units of $\hbar = 1$)

$$[S_{i+}, S_{i-}] = 2S, \quad [S_{i+}, S_{iz}] = -S_{i+}, \quad \text{and} \quad [S_{i-}, S_{iz}] = S_{i-}, \quad (3.5)$$

with the first commutator is shifted from the actual spin commutator $[S_{i+}, S_{i-}] = 2S_{iz}$. This difference in the commutators can be ignored in different instances, for example when magnon-magnon interaction is negligible. However, in some case this is not true as was shown recently in $\text{Yb}_2\text{Ti}_2\text{O}_7$ where higher order interactions are necessary for fully describing the low energy excitations in this magnet [5]. The latter interaction is beyond the scope of this work and we will be only dealing with the harmonic approximation and study Hamiltonians that are quadratic in $\{a_i^\dagger, a_i\}$.

The starting point of constructing the magnon Hamiltonian is to choose a reference frame $\{x'_i, y'_i, z'_i\}$ such that when the system is in its zero-temperature ordered magnetic state the spins at the local RE sites point along the local z'_i direction. To do this, let Q_i be a 3×3 orthogonal matrix that relates the old reference frame $\{x_i, y_i, z_i\}$ defined in Appendix B to the new local frame,

$$\begin{pmatrix} x_i \\ y_i \\ z_i \end{pmatrix} = Q_i \begin{pmatrix} x'_i \\ y'_i \\ z'_i \end{pmatrix}. \quad (3.6)$$

This will be reflected in the exchange Hamiltonian by transforming the exchange matrix \mathcal{J}_{ij} to $\tilde{\mathcal{J}}_{ij}$, giving

$$\mathcal{H}_{\text{ex}} = \sum_{\langle ij \rangle} \tilde{S}_i^T \tilde{\mathcal{J}}_{ij} \tilde{S}_j, \quad (3.7)$$

where $\tilde{\mathcal{J}}_{ij} = Q_i^T \mathcal{J}_{ij} Q_j$ with \mathcal{J}_{ij} is defined in Eq. (2.11), and $\tilde{S}_i = Q_i^T S_i$ defines the spin in the new reference frame. This will also affect the Zeeman term giving

$$\mathcal{H}_Z = - \sum_i \tilde{B}_i^T \tilde{g}_i \tilde{S}_i, \quad (3.8)$$

where $\vec{B}_i = Q_i^T \vec{B}_i$ is the applied magnetic field at site i expressed in the new reference frame, and $\tilde{g}_i = Q_i^T g Q_i$ the g -tensor in the primed coordinates.

3.1 Magnetic Order in the RE Pyrochlores

There are different types of magnetic order that can occur in the RE pyrochlore systems as discussed in Chapter 1. To define the different possible types of ordering, we begin by introducing the basis vectors of the irreducible representations of the octahedral space group [41]:

$$m_{A_2} = S_{1z} + S_{2z} + S_{3z} + S_{4z}, \quad (3.9)$$

$$m_{E^\pm} = S_{1\pm} + S_{2\pm} + S_{3\pm} + S_{4\pm}, \quad (3.10)$$

$$m_{T_{1,1}} = \begin{pmatrix} m_{T_{1,1},x} \\ m_{T_{1,1},y} \\ m_{T_{1,1},z} \end{pmatrix} = \begin{pmatrix} S_{1z} - S_{2z} - S_{3z} + S_{4z} \\ S_{1z} - S_{2z} + S_{3z} - S_{4z} \\ S_{1z} + S_{2z} - S_{3z} - S_{4z} \end{pmatrix}, \quad (3.11)$$

$$m_{T_{1,2}} = \begin{pmatrix} m_{T_{1,2},x} \\ m_{T_{1,2},y} \\ m_{T_{1,2},z} \end{pmatrix} = \begin{pmatrix} \frac{1}{2}\epsilon^* (S_{1+} - S_{2+} - S_{3+} + S_{4+}) + \text{h.c.} \\ \frac{1}{2}\epsilon (S_{1+} - S_{2+} + S_{3+} - S_{4+}) + \text{h.c.} \\ S_{1x} + S_{2x} - S_{3x} - S_{4x} \end{pmatrix}, \quad (3.12)$$

$$m_{T_2} = \begin{pmatrix} m_{T_2,x} \\ m_{T_2,y} \\ m_{T_2,z} \end{pmatrix} = \begin{pmatrix} -\frac{i}{2}\epsilon^* (S_{1+} - S_{2+} - S_{3+} + S_{4+}) + \text{h.c.} \\ -\frac{i}{2}\epsilon (S_{1+} - S_{2+} + S_{3+} - S_{4+}) + \text{h.c.} \\ S_{1y} + S_{2y} - S_{3y} - S_{4y} \end{pmatrix}, \quad (3.13)$$

where $\epsilon = \exp(2\pi i/3)$, and the spins represent the expectation values not the operators for the above expressions to define the order parameters. The above order parameters are classified as follows. The basis vectors $\{m_{T_{1,1}}, m_{T_{1,2}}\}$ defines the colinear and noncolinear ferromagnetic states, respectively, while the other three order

parameters represent different types of AFM orderings with m_{A_2} representing the “all in-all out”, m_{E^\pm} defines the noncolinear noncoplanar state (referred as ψ_2 [41]) plus the noncolinear coplanar state labeled by ψ_3 , and finally m_{T_2} introduces the last type of AFM which is known by Palmer-Chalker (PC) states [42]. For completeness, we would like to express the anisotropic exchange Hamiltonian defined in Eqs. (2.4), (2.5), (2.6), and (2.7) in terms of the above basis vectors[41]

$$X_1 = -\frac{1}{8}m_{A_2}^2 + \frac{1}{24}m_{T_{1,1}}^2, \quad (3.14)$$

$$X_2 = -\frac{\sqrt{2}}{3}m_{T_{1,1}} \cdot m_{T_{1,2}}, \quad (3.15)$$

$$X_3 = \frac{1}{6} \left(m_{T_{1,2}}^2 - m_{T_2}^2 \right), \quad (3.16)$$

$$X_4 = -\frac{1}{8}m_{E^+} m_{E^-} + \frac{1}{24}m_{T_{1,2}}^2 + \frac{1}{24}m_{T_2}^2. \quad (3.17)$$

In the next sections we will study three QREP systems with different magnetic order.

3.2 All In-all Out State in $\text{Nd}_2\text{Zr}_2\text{O}_7$

The QREP $\text{Nd}_2\text{Zr}_2\text{O}_7$ has GSD that belongs to the $\Gamma_{5,6}$ category. This magnet orders antiferromagnetically in an all in-all out (AIAO) state below 0.285 K [22]. In addition, $\text{Nd}_2\text{Zr}_2\text{O}_7$ was shown to be a magnetic moment fragmentation candidate where the fragmentation was observed to occur below 0.7 K as verified experimentally and explained theoretically [22, 23]. The starting point for calculating the energy dispersions of magnons in $\text{Nd}_2\text{Zr}_2\text{O}_7$ is the effective exchange Hamiltonian defined in Eq. (2.26). We apply the HP transformation defined in Eq. (3.4) on the spin operators giving

$$\mathcal{H}_{\text{ex}}^{\Gamma_{5,6}} \approx \mathcal{H}^0 + \sum_{\langle ij \rangle} \left[-\frac{\tilde{J}_{zz}}{2} (a_i^\dagger a_i + a_j^\dagger a_j) + \rho^+ (a_i a_j^\dagger + \text{h.c.}) + \rho^- (a_i a_j + \text{h.c.}) \right], \quad (3.18)$$

where $\mathcal{H}^0 = \sum_{\langle ij \rangle} \frac{\tilde{J}_{zz}}{4}$, $\rho^\pm = \frac{\tilde{J}_{xx} \pm J_{yy}}{4}$, and h.c. stands for the Hermitian conjugate. The next step is to Fourier transform the bosonic operators as follows

$$a_{nj} = \frac{1}{\sqrt{N}} \sum_k e^{-i\vec{k} \cdot \vec{r}_{nj}} a_j(k), \quad a_{nj}^\dagger = \frac{1}{\sqrt{N}} \sum_k e^{i\vec{k} \cdot \vec{r}_{nj}} a_j^\dagger(k), \quad (3.19)$$

where N is the total number of magnetic ions, n labels the tetrahedra, and $\vec{r}_{nj} = \vec{r}_n + \vec{r}_j$ is the position of the j^{th} ion located in the n^{th} tetrahedron. The above transformations are subject to the orthogonality relation $\sum_n e^{i(\vec{k} - \vec{k}') \cdot \vec{r}_n} = N \delta_{\vec{k}, \vec{k}'}$. Using the above transformations back in Eq. (3.18), we get

$$\mathcal{H}_{\text{ex}}^{\Gamma_{5,6}} = \tilde{\mathcal{H}}^0 + \sum_k L_k^\dagger M(k) L_k, \quad (3.20)$$

where $\tilde{\mathcal{H}}^0 = \frac{1}{4} \sum_{\langle ij \rangle} \tilde{J}_{zz} = \frac{9}{4} N \tilde{J}_{zz}$,

$$L_k = \left[a_1(k) \ a_2(k) \ a_3(k) \ a_4(k) \ a_1(-k) \ a_2(-k) \ a_3(-k) \ a_4(-k) \right]^T, \quad (3.21)$$

and $M(k) = \begin{pmatrix} A(k) & B(k) \\ B(k) & A(k) \end{pmatrix}$. $A(k)$ and $B(k)$ are 4×4 matrices,

$$A(k) = \left(\frac{\tilde{J}_{xx} + J_{yy}}{2} \right) R(k) - 3\tilde{J}_{zz}\mathbb{1}, \quad B(k) = \left(\frac{\tilde{J}_{xx} - J_{yy}}{2} \right) R(k), \quad (3.22)$$

where $R_{ij}(k) = \cos[\vec{k} \cdot (\vec{r}_i - \vec{r}_j)] - \delta_{ij}$. Thus, we have constructed the quadratic bosonic Hamiltonian in k -space for the $\Gamma_{5,6}$ ground state doublet (GSD). In the presence of an external magnetic field, the Zeeman Hamiltonian for this case takes the form

$$\mathcal{H}_Z^{\Gamma_{5,6}} = -\mu_B \sum_i B_{iz} g_{\parallel} S_{iz} = -\mu_B \sum_i B_{iz} g_{\parallel} \left[\sin \theta \tilde{S}_{ix} + \cos \theta \tilde{S}_{iz} \right], \quad (3.23)$$

where θ is defined in Eq. (2.25). Note that this is only true if the spins are pointing along the local \tilde{z} axis. However, in the case of higher magnetic fields, the spins will deviate from their local \tilde{z} towards the direction of the applied field [43]. In this case, one needs to include the canting angle by performing coordinate transformation such that the local z of the new frame points along the spin directions. In this work, we will

only consider the AIAO state with low fields and in this case the effective quadratic Hamiltonian will have the form of Eq. (3.20) with A given by

$$A_{ij}(k) = \left(\frac{\tilde{J}_{xx} + J_{yy}}{2} \right) R_{ij}(k) + (\Delta_i - 3\tilde{J}_{zz})\delta_{ij}, \quad (3.24)$$

where $\Delta_i = \mu_B B_{iz} g_{\parallel} \cos \theta$. If we consider the applied magnetic field in the [111] crystallographic direction, then in the local frame of the four RE sites (defined in Appendix B) the magnetic field is

$$\vec{B}_1 = B\hat{z}_1, \quad (3.25)$$

$$\vec{B}_2 = -\frac{4B}{3\sqrt{2}}\hat{x}_2 - \frac{B}{3}\hat{z}_3, \quad (3.26)$$

$$\vec{B}_3 = \frac{\sqrt{2}B}{3}\hat{x}_3 + \sqrt{\frac{2}{3}}B\hat{y}_3 - \frac{B}{3}\hat{z}_3, \quad (3.27)$$

$$\vec{B}_4 = \frac{\sqrt{2}B}{3}\hat{x}_4 - \sqrt{\frac{2}{3}}B\hat{y}_4 - \frac{B}{3}\hat{z}_4. \quad (3.28)$$

Thus, we have $\Delta_1 = \mu_B B g_{\parallel} \cos \theta$, and $\Delta_2 = \Delta_3 = \Delta_4 = -\frac{\Delta_1}{3}$. The diagonalization of the exchange Hamiltonian Eq. (3.20) is done analytically in the next chapter. Different attempts have been carried out to determine the exchange constants and the values of the g -tensor components for $\text{Nd}_2\text{Zr}_2\text{O}_7$ as summarized in Table 3.1.

Table 3.1: Sets of values of the exchange parameters, the components of the g -tensor, and the rotation angle θ of $\text{Nd}_2\text{Zr}_2\text{O}_7$ obtained in four different studies [22, 23, 43, 44].

Ref.	\tilde{J}_{xx} (meV)	J_{yy} (meV)	\tilde{J}_{zz} (meV)	g_{\perp}	g_{\parallel}	θ (rad)
[22]	-0.047	0	0.103	0	4.5	0
[23]	0.103	0	-0.047	-	-	0.83
[44]	0.086	0.006	-0.043	0	4.55	1.26
[43]	0.091	0.014	-0.046	0	5.0	0.98

3.3 Anti-ferromagnetic Ordering in $\text{Er}_2\text{Ti}_2\text{O}_7$

It was found that $\text{Er}_2\text{Ti}_2\text{O}_7$ orders in an antiferromagnetic (AFM) state below 1.2 K [17, 18, 19]. This AFM state is due to order by quantum disorder [17, 19]. The

exchange constants and the g -tensor components for this material are listed in Table 3.2. Considering the Ψ_2 AFM state [20], the magnetic moments of the Er^{+3} ions in the primitive unit cell are

$$\vec{S}_1 = \frac{S}{2\sqrt{6}}(-2, 1, 1), \quad \vec{S}_2 = \frac{S}{2\sqrt{6}}(2, -1, 1), \quad (3.29)$$

$$\vec{S}_3 = \frac{S}{2\sqrt{6}}(2, 1, -1), \quad \vec{S}_4 = \frac{S}{2\sqrt{6}}(-2, -1, -1), \quad (3.30)$$

where the above spins are represented with respect to the cubic (global) axes. In the local coordinates, the four spins point along the \hat{x} direction. We now define a coordinate system \vec{r}'_i in which the spins will point locally along z'_i . In this simple case the transformation matrix (Eq. (3.6)) is

$$Q_i = \begin{pmatrix} 0 & 0 & 1 \\ 1 & 0 & 0 \\ 0 & 1 & 0 \end{pmatrix}; \quad i \in \{1, 2, 3, 4\}. \quad (3.31)$$

We first apply the above transformation on the exchange Hamiltonian and then use the HP transformation on the operators \tilde{S}_i . Keeping only quadratic terms in the bosonic operators, we get

$$\mathcal{H}_{ex} \approx \mathcal{H}^0 + \sum_{\langle ij \rangle} \left[\rho_{ij} a_i^\dagger a_j^\dagger + \rho_{ij}^* a_i a_j + \sigma_{ij} a_i^\dagger a_j + \sigma_{ij}^* a_i a_j^\dagger - \frac{\tilde{\mathcal{J}}_{ij}^{zz}}{2} (a_i^\dagger a_i + a_j^\dagger a_j) \right], \quad (3.32)$$

where

$$\rho_{ij} = \frac{1}{4} \left[\tilde{\mathcal{J}}_{(ij)}^{xx} + i(\tilde{\mathcal{J}}_{(ij)}^{xy} + \tilde{\mathcal{J}}_{(ij)}^{yx}) - \tilde{\mathcal{J}}_{(ij)}^{yy} \right], \quad (3.33)$$

$$\sigma_{ij} = \frac{1}{4} \left[\tilde{\mathcal{J}}_{(ij)}^{xx} - i(\tilde{\mathcal{J}}_{(ij)}^{xy} - \tilde{\mathcal{J}}_{(ij)}^{yx}) + \tilde{\mathcal{J}}_{(ij)}^{yy} \right], \quad (3.34)$$

and $\tilde{\mathcal{J}}_{ij} = Q_i^T \mathcal{J}_{ij} Q_j$. Using Eq. (3.19), we transform the above Hamiltonian into k -space,

$$\mathcal{H}_{ex}^{\text{Er}} = \tilde{\mathcal{H}}_0^{\text{Er}} + \sum_k L_k^\dagger M(k) L_k, \quad (3.35)$$

where $M(k) = \begin{pmatrix} A(k) & B(k) \\ B^*(k) & A(k) \end{pmatrix}$. The 4×4 matrices A and B are

$$A_{ij}(k) = 2\sigma_{ij} \cos \left[\vec{k} \cdot (\vec{r}_i - \vec{r}_j) \right] - \sum_{\ell} \tilde{J}_{i\ell}^{zz} \delta_{ij}, \quad (3.36)$$

$$B_{ij}(k) = 2\rho_{ij} \cos \left[\vec{k} \cdot (\vec{r}_i - \vec{r}_j) \right]. \quad (3.37)$$

In the presence of external magnetic field, one has to include the Zeeman Hamiltonian which will only shift the diagonal entries of $M(k)$. In this case, we should be very careful about the spin directions as the external field will tend to tilt the spins from their ψ_2 state towards the field direction. Depending on the strength and direction of the field, the canting direction will be different and thus different dispersions. If we assume that magnetic field has been applied along $[1\bar{1}0]$ which was high enough to polarize the spin along its direction. In this case, the quadratic bosonic Hamiltonian will have the same form as Eq. (3.35) but with $M(k) \rightarrow M(k) + \mathcal{X}$, where $\mathcal{X} = \mu_B B \begin{pmatrix} \Delta & 0 \\ 0 & \Delta \end{pmatrix}$, and Δ is the following 4×4 matrix

$$\Delta = \begin{pmatrix} g_{\perp} & 0 & 0 & 0 \\ 0 & g_{\perp} & 0 & 0 \\ 0 & 0 & \frac{g_{\perp}}{3} + \frac{2g_{\parallel}}{3} & 0 \\ 0 & 0 & 0 & \frac{g_{\perp}}{3} + \frac{2g_{\parallel}}{3} \end{pmatrix}. \quad (3.38)$$

The process of obtaining the energy bands and the corresponding normal modes is discussed in the next chapter in more details. In the next section, we will construct the the quadratic bosonic Hamiltonian for the third example of a RE magnet $\text{Yb}_2\text{Ti}_2\text{O}_7$.

Table 3.2: The values for the four exchange parameters and the components of the g -tensor for $\text{Er}_2\text{Ti}_2\text{O}_7$ [25].

Ref.	J_{zz}	J_{\pm}	$J_{\pm\pm}$	$J_{z\pm}$	g_{\perp}	g_{\parallel}
[25]	-0.025	0.065	0.042	-0.0088	5.97	2.45

3.4 Ferromagnetic Ordering in $\text{Yb}_2\text{Ti}_2\text{O}_7$

The RE pyrochlore magnet $\text{Yb}_2\text{Ti}_2\text{O}_7$ is one of the most studied systems among the pyrochlores [5, 15, 16, 48, 50]. This material orders ferromagnetically at temperature near 0.2 K as verified by different experiments [5, 15, 16, 36]. Different experiments to obtain the values of the exchange parameters are summarized in Table 3.3, however the recent results by Thompson, *et al.* [5] are the most reliable as they incorporate old and new data obtained in these experiments. Recent experiments have shown that $\text{Yb}_2\text{Ti}_2\text{O}_7$ has strong quantum fluctuations at low fields making it a potential candidate for a quantum spin liquid (QSL). The recently obtained values of the exchange parameters place $\text{Yb}_2\text{Ti}_2\text{O}_7$ close to the boundary between the FM state and the anti-ferromagnetic ordering observed in $\text{Er}_2\text{Ti}_2\text{O}_7$ [20], which is thought to be an indication of the strong quantum fluctuations in this material are also reflected in the exchange parameters, among which $J_{z\pm}$ has the highest value according to the work of Thompson *et al.* [5].

Table 3.3: Sets of values of the four exchange parameters of $\text{Yb}_2\text{Ti}_2\text{O}_7$ obtained in different experiments.

Ref.	J_{zz}	J_{\pm}	$J_{\pm\pm}$	$J_{z\pm}$	g_{\perp}	g_{\parallel}
[36]	0.17 ± 0.04	0.05 ± 0.01	0.05 ± 0.01	-0.14 ± 0.01	4.32	1.80
[37]	0.07	0.085	0.04	-0.15	4.09	2.06
[5]	0.026 ± 0.003	0.074 ± 0.002	0.048 ± 0.002	-0.159 ± 0.002	4.17 ± 0.02	2.14 ± 0.03

In this work, we consider an applied field along $[1\bar{1}0]$ with the spins at the four basis sites aligned with the field [36]. In the local frame, the spin expectation values for the RE sites are

$$\vec{S}_1 = \frac{1}{2}(0, -1, 0), \quad \vec{S}_2 = \frac{1}{2}(0, 1, 0), \quad (3.39)$$

$$\vec{S}_3 = \frac{1}{2}\left(-\frac{1}{\sqrt{3}}, 0, -\sqrt{\frac{2}{3}}\right), \quad \vec{S}_4 = \frac{1}{2}\left(\frac{1}{\sqrt{3}}, 0, \sqrt{\frac{2}{3}}\right). \quad (3.40)$$

Thus, the Q_i matrix for sites 1 and 2 are given below

$$Q_1 = \begin{pmatrix} 1 & 0 & 0 \\ 0 & 0 & -1 \\ 0 & 1 & 0 \end{pmatrix}, \quad (3.41)$$

$$Q_2 = \begin{pmatrix} 1 & 0 & 0 \\ 0 & 0 & 1 \\ 0 & -1 & 0 \end{pmatrix}. \quad (3.42)$$

However, for sites 3 and 4 one needs to do a rotation in the local xz -plane such that the z axis points along the spin directions (i.e. along the applied magnetic field). Consequently, the Q_i matrix for the latter sites are

$$Q_3 = \begin{pmatrix} -\sqrt{\frac{2}{3}} & 0 & -\frac{1}{\sqrt{3}} \\ 0 & 1 & 0 \\ \frac{1}{\sqrt{3}} & 0 & -\sqrt{\frac{2}{3}} \end{pmatrix}, \quad (3.43)$$

$$Q_4 = \begin{pmatrix} \sqrt{\frac{2}{3}} & 0 & \frac{1}{\sqrt{3}} \\ 0 & 1 & 0 \\ -\frac{1}{\sqrt{3}} & 0 & \sqrt{\frac{2}{3}} \end{pmatrix}. \quad (3.44)$$

Therefore, the effective quadratic Hamiltonian (exchange plus Zeeman) in this case is

$$\mathcal{H}_{\text{eff}}^{\text{Yb}} = \tilde{\mathcal{H}}_0^{\text{Yb}} + \sum_k L_k^\dagger M(k) L_k, \quad (3.45)$$

where $M(k) = \begin{pmatrix} A(k) & B(k) \\ B^*(k) & A(k) \end{pmatrix} + \mu_B B \mathcal{M}$ with $\mathcal{M} = \begin{pmatrix} \Delta & 0 \\ 0 & \Delta \end{pmatrix}$, and Δ is the following 4×4 matrix

$$\Delta = \begin{pmatrix} g_\perp & 0 & 0 & 0 \\ 0 & g_\perp & 0 & 0 \\ 0 & 0 & \frac{g_\perp}{3} + \frac{2g_\parallel}{3} & 0 \\ 0 & 0 & 0 & \frac{g_\perp}{3} + \frac{2g_\parallel}{3} \end{pmatrix}. \quad (3.46)$$

The calculations of magnons dispersions for this case will be discussed in the next chapter.

3.5 Summary

We have calculated the quadratic magnon Hamiltonian for the all in-all out ordered state in $\text{Nd}_2\text{Zr}_2\text{O}_7$, the AFM (Ψ_2) state in $\text{Er}_2\text{Ti}_2\text{O}_7$, and the FM ordering in $\text{Yb}_2\text{Ti}_2\text{O}_7$ in the presence of magnetic field. One can follow the same procedure to study systems with any other type of magnetic ordering by performing the required transformations. An important point one has to consider is the canting angle in the presence of external magnetic field. The knowledge of this angle will be very important in determining accurate energy dispersions. In the next chapter we will calculate the corresponding energy dispersions analytically, and discuss the calculations of the normal modes and the Bogoliubov transformation in these systems.

Chapter 4

Results and discussion: Energy bands and normal mode calculations

An important task in studying magnons in QREPs is to diagonalize the quadratic Hamiltonians in Eqs. (3.20), (3.35), and (3.45), which will provide us with the energy bands and the associated normal modes. With these, one can calculate different physical quantities such as the thermodynamic quantities and the structure factor. [20, 23, 47]. The starting point is to use Bogoliubov transformation to diagonalize the 8×8 matrix $M(k)$ giving

$$\mathcal{H}_{ex} = \mathcal{H}_0 + \sum_k \mathcal{L}_k^\dagger \mathcal{M}(k) \mathcal{L}_k, \quad (4.1)$$

where $\mathcal{L}_k = Z(k)L_k$. $Z(k)$ is the Bogoliubov transformation matrix, and

$$\mathcal{M}(k) = Z^\dagger(k)M(k)Z(k) = \begin{pmatrix} \mathcal{E} & 0 \\ 0 & \mathcal{E} \end{pmatrix}, \quad (4.2)$$

where $\mathcal{E}_{ij} = \varepsilon_i(\vec{k})\delta_{ij}$. The column vector \mathcal{L}_k contains the transformed bosonic operators which must preserve the usual commutation relations for bosons as defined in Eq. (3.2) which will add a constraint on the matrix $Z(k)$. The bosonic commutation

relation is

$$L_k L_k^\dagger - (L_k^* L_k^T)^T = \mathcal{G} = \begin{pmatrix} \mathbb{1} & 0 \\ 0 & -\mathbb{1} \end{pmatrix}, \quad (4.3)$$

where L_k^* stands for the column vector of the adjoint bosonic operators of L_k , and $\mathbb{1}$ is the 4×4 identity matrix. The column of operators \mathcal{L}_k must also satisfy the relation above which results in the following condition for the Bogoliubov matrix

$$Z(k) \mathcal{G} Z^\dagger(k) = \mathcal{G}. \quad (4.4)$$

Thus, the energy dispersions and the normal modes are obtained by solving simultaneously Eqs. (4.2) and (4.4) for $Z(k)$ and $\mathcal{E}(k)$. To calculate the energy dispersions, we combine Eqs. (4.2) and (4.4) giving

$$Z^{-1} \mathcal{G} M(k) Z = \mathcal{G} \mathcal{M}(k) = \begin{pmatrix} \mathcal{E} & 0 \\ 0 & -\mathcal{E} \end{pmatrix}. \quad (4.5)$$

Consequently, the energy dispersions of magnons are extracted from the eigenvalues of the non-Hermitian matrix $\mathcal{G} M(k)$ Eq. (4.5). Since the eigenvalues of $\mathcal{G} M(k)$ will have the form $\pm \varepsilon_i(\vec{k})$, the characteristic polynomial of this matrix must be quartic in $\varepsilon^2(\vec{k})$ and is generally written as

$$(\varepsilon^2)^4 + \xi_6(k)(\varepsilon^2)^3 + \xi_4(k)(\varepsilon^2)^2 + \xi_2(k)\varepsilon^2 + \det[\mathcal{G} M] = 0, \quad (4.6)$$

where the coefficients $\{\xi_2(k), \xi_4(k), \xi_6(k)\}$ are the coefficients of the characteristic polynomial of $\mathcal{G} M$. The latter coefficients can be found analytically and thus the analytic form of the energy dispersions is always possible for this kind of problem and it is

$$\varepsilon(\vec{k}) = \sqrt{-\frac{\xi_6(\vec{k})}{4} \pm \mathcal{S}(\vec{k}) \pm \frac{1}{2} \sqrt{-4\mathcal{S}^2(\vec{k}) - 2P(\vec{k}) \mp \frac{Q(\vec{k})}{\mathcal{S}(\vec{k})}}}, \quad (4.7)$$

where $\{S(k), P(k), Q(k)\}$ are calculated in Appendix D. On the other hand, an analytic calculation of the Bogoliubov matrix is not always possible and thus we rely on the numerical methods in most cases (see Appendix E). In the next section, we will apply the above procedure to calculate the energy dispersions of magnons within the harmonic approximation for the three QREPs mentioned in the previous chapter. We also found that the matrix $Z(k)$ can be calculated analytically for the $\Gamma_{5,6}$ GSD as

mentioned in the next section. However, for the other cases one should rely on the numerical procedure described in Appendix E.

4.1 Exact Analytic Diagonalization of $\mathcal{H}_{\text{ex}}^{\Gamma_{5,6}}$

In this section, we will first consider two special cases of Eq. (3.22): (1) $\tilde{J}_{xx} = 0$ or $J_{yy} = 0$, and (2) $\tilde{J}_{yy} = \tilde{J}_{xx}$. Then we will solve the general case with no constraints on the exchange parameters. In addition to the zero field cases, we will consider the case with magnetic field along the [111] cubic direction in the last subsection. Before starting the four subsections, we introduce the following unitary transformation

$$\mathcal{U} = \frac{1}{\sqrt{2}} \begin{pmatrix} \mathbb{1} & \mathbb{1} \\ -\mathbb{1} & \mathbb{1} \end{pmatrix}. \quad (4.8)$$

Applying the above unitary transformation on $\mathcal{G}M(k)$, we get

$$\mathcal{U}^\dagger \mathcal{G}M(k) \mathcal{U} = \begin{pmatrix} 0 & A+B \\ A-B & 0 \end{pmatrix}. \quad (4.9)$$

Since \mathcal{U} is unitary, one can easily show that $\mathcal{G}M(k)$ and $\mathcal{U}^\dagger \mathcal{G}M(k) \mathcal{U}$ share the same eigenvalues. Thus, the eigenvalue equation is

$$\begin{vmatrix} \lambda \mathbb{1} & A+B \\ A-B & \lambda \mathbb{1} \end{vmatrix} = |(A^2 - B^2) - \lambda^2 \mathbb{1}| = 0. \quad (4.10)$$

Consequently, the problem reduces to finding the eigenvalues of the 4×4 matrix $A^2 - B^2$ which will be done for each case. Moreover, if \vec{Y} is an eigenvector of $\mathcal{U}^\dagger \mathcal{G}M(k) \mathcal{U}$ then $\mathcal{U} \vec{Y}$ is an eigenvector of $\mathcal{G}M(k)$ with the same eigenvalue. The Bogoliubov matrix $Z(k)$ can be found analytically for each case as will be discussed next.

4.1.1 Case I: $\tilde{J}_{xx} = 0$ or $J_{yy} = 0$

Without loss of generality, let us consider the case when $J_{yy} = 0$. Using Eq. 4.10 together with Eq. (3.22), we obtain the following equation for the energy dispersion,

$$\left| R - \frac{9\tilde{J}_{zz} - \varepsilon^2}{3\tilde{J}_{xx}\tilde{J}_{zz}} \right| = 0, \quad (4.11)$$

where R is the 4×4 matrix defined in Eq. (C.1). Thus, we only need the eigenvalues of R from which we can find the corresponding energy dispersions. After lengthy calculations of the eigenvalues of R (in Appendix C) and by using Eq. (4.11), we find that the system has a doubly degenerate flat band with energy

$$\varepsilon_{1,2}(\vec{k}) = \sqrt{3\tilde{J}_{zz}(3\tilde{J}_{zz} + \tilde{J}_{xx})}, \quad (4.12)$$

and two other dispersive bands,

$$\varepsilon_{3,4}(\vec{k}) = \sqrt{9\tilde{J}_{zz}^2 - 3\tilde{J}_{zz}\tilde{J}_{xx}r_{\pm}}, \quad (4.13)$$

where r_{\pm} is given in Eq. C.2. This case applies to the rare-earth pyrochlore $\text{Nd}_2\text{Zr}_2\text{O}_7$ with the exchange parameters extracted from [23] (see Table 3.1). The energy dispersions of magnons in $\text{Nd}_2\text{Zr}_2\text{O}_7$ through different symmetry directions are plotted in Figure 4.1. Note that the appearance of the doubly degenerate flat in $\text{Nd}_2\text{Zr}_2\text{O}_7$ was also verified experimentally and theoretically in different studies [22, 23, 43, 44], and this feature is also generic for different pyrochlore systems and was also found in the electronic band structure for the nearest-neighbor hopping model with no spin flipping [45, 46]. On the other hand, two other sets of exchange parameters for this material have been extracted recently in [43, 44], with nonzero J_{yy} which is smaller than the other contributions (see Table 3.1). The treatment of the latter sets of exchange parameters is given in Section 4.1.3.

Aside from the energy dispersions, we are interested in finding the Bogoliubov transformation matrix for this case in order to have full knowledge of the diagonalized Hamiltonian as it might be important when calculating some physical quantities such as the dynamical structure factor [20, 49]. Here, we follow the procedure of Appendix

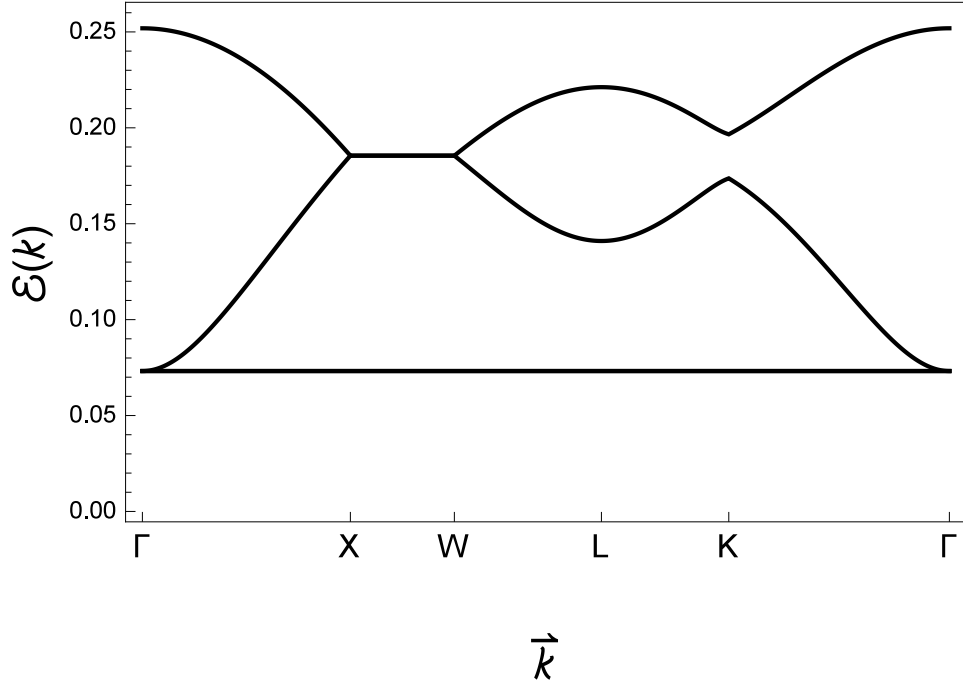


Figure 4.1: Energy bands of magnons in $\text{Nd}_2\text{Zr}_2\text{O}_7$ at zero magnetic field with exchange constants taken from Ref. [23].

E, where we find the eigenvectors of $\mathcal{G}M(k)$ as follows. First, we observe that

$$\mathcal{U}\mathcal{G}M\mathcal{U}^\dagger = \begin{pmatrix} 0 & 3\tilde{J}_{zz}\mathbb{1} \\ -\tilde{J}_{xx}R + 3\tilde{J}_{zz}\mathbb{1} & 0 \end{pmatrix}, \quad (4.14)$$

where \mathcal{U} is given in Eq. (4.8). We assume that \vec{X} is an eigenvector of $\mathcal{U}\mathcal{G}M\mathcal{U}^\dagger$, with eigenvalue ε_x , that is expressed in the following block form

$$\vec{X} = \begin{pmatrix} \vec{u} \\ \vec{v} \end{pmatrix}. \quad (4.15)$$

By simple algebra, with the use of Eq. 4.14, we have

$$\vec{v} = \frac{\varepsilon_x}{3\tilde{J}_z}\vec{u}, \quad (4.16)$$

$$\left[-\tilde{J}_x R + 3\tilde{J}_z\mathbb{1}\right]\vec{u} = \varepsilon_x\vec{v}. \quad (4.17)$$

By eliminating \vec{v} , we have

$$R\vec{u} = \frac{9\tilde{J}_z^2 - \varepsilon_x^2}{3\tilde{J}_x\tilde{J}_z}\vec{u}. \quad (4.18)$$

Thus, \vec{u} is an eigenvector of R with eigenvalue $\frac{9\tilde{J}_z^2 - \varepsilon_x^2}{3\tilde{J}_x\tilde{J}_z}$. In this way, we have

$$\vec{X} = \frac{1}{\sqrt{1 + \left(\frac{\varepsilon_x}{3\tilde{J}_z}\right)^2}} \begin{pmatrix} \vec{u} \\ \frac{\varepsilon_x}{3\tilde{J}_z}\vec{u} \end{pmatrix}. \quad (4.19)$$

Note that the other four eigenvectors are found by the simple replacement $\varepsilon_x \rightarrow -\varepsilon_x$. Consequently, we find the normalized eigenvectors of $\mathcal{G}M$ to be

$$\vec{X} = \mathcal{U}^\dagger \vec{X} = \frac{1}{\sqrt{2 + 2\left(\frac{\varepsilon_x}{3\tilde{J}_z}\right)^2}} \begin{pmatrix} \left(1 - \frac{\varepsilon_x}{3\tilde{J}_z}\right)\vec{u} \\ \left(1 + \frac{\varepsilon_x}{3\tilde{J}_z}\right)\vec{u} \end{pmatrix}. \quad (4.20)$$

Thus, we have obtained an analytic form of the matrix \tilde{Z} . To find the full Bogoliubov matrix Z , we are left with finding the block diagonal matrix P such that $Z = \tilde{Z}P$. Without loss of generality, we assume that the system is only degenerate in the flat bands, i.e. the matrix $\mathcal{G}M$ has 6 distinct eigenvalues where two of them are doubly degenerate, giving the total eight eigenvalues of the latter matrix. Thus, the matrix P has six blocks where two of them are 2×2 and the rest are 1×1 . Starting with the positive energy sector of $\mathcal{G}M$, the 2×2 blocks are

$$W_1 = -\frac{3}{2} \begin{bmatrix} \tilde{J}_z & \varepsilon_1 \\ \varepsilon_1 & 9\tilde{J}_z \end{bmatrix} \mathbb{1}. \quad (4.21)$$

The other two 1×1 matrices in the positive energy sector are

$$W_2 = -\frac{3}{2} \begin{bmatrix} \tilde{J}_z & \varepsilon_3 \\ \varepsilon_3 & 9\tilde{J}_z \end{bmatrix}, \quad (4.22)$$

$$W_3 = -\frac{3}{2} \begin{bmatrix} \tilde{J}_z & \varepsilon_4 \\ \varepsilon_4 & 9\tilde{J}_z \end{bmatrix}. \quad (4.23)$$

However, for the negative energy sector, we only use the map $\varepsilon_i \rightarrow -\varepsilon_i$, giving

$$W_4 = \frac{3}{2} \left[\frac{\tilde{J}_z}{\varepsilon_1} + \frac{\varepsilon_1}{9\tilde{J}_z} \right] \mathbb{1}, \quad (4.24)$$

$$W_5 = \frac{3}{2} \left[\frac{\tilde{J}_z}{\varepsilon_3} + \frac{\varepsilon_3}{9\tilde{J}_z} \right], \quad (4.25)$$

$$W_6 = \frac{3}{2} \left[\frac{\tilde{J}_z}{\varepsilon_4} + \frac{\varepsilon_4}{9\tilde{J}_z} \right]. \quad (4.26)$$

Consequently, we have

$$P = \text{diag} \left[\sqrt{W_1}, \sqrt{W_2}, \sqrt{W_3}, \sqrt{-W_4}, \sqrt{-W_5}, \sqrt{-W_6} \right]. \quad (4.27)$$

To conclude this section, we have obtained the analytic results of the energy dispersions and normal modes for the case when $J_{yy} = 0$ within the LSWA. We would like now to proceed with the other cases in the next sections and calculate the energy bands and the Bogoliubov matrix in each case.

4.1.2 Case II: $\tilde{J}_{xx} = J_{yy}$

In this interesting case, we have the blocks $B = 0$ (where 0 is the 4×4 zero matrix). Consequently, the eigenvalue equation for this case is

$$|A^2 - \lambda^2 \mathbb{1}| = |A - \lambda \mathbb{1}| \times |A + \lambda \mathbb{1}| = 0. \quad (4.28)$$

Using Eq. (3.22) together with the eigenvalues of R in Eq. (C.2), we obtain the following energy dispersions for this case

$$\varepsilon_{1,2}(\vec{k}) = |3\tilde{J}_{zz} + \tilde{J}_{xx}|, \quad (4.29)$$

$$\varepsilon_{3,4}(\vec{k}) = |\tilde{J}_{xx} r_{\pm} - 3\tilde{J}_{zz}|. \quad (4.30)$$

We plot the energy dispersions for the case with $\tilde{J}_{xx} = J_{yy} = -0.25$ and $\tilde{J}_{zz} = -0.1$ in Figure 4.2. The Bogoliubov matrix takes the following general form

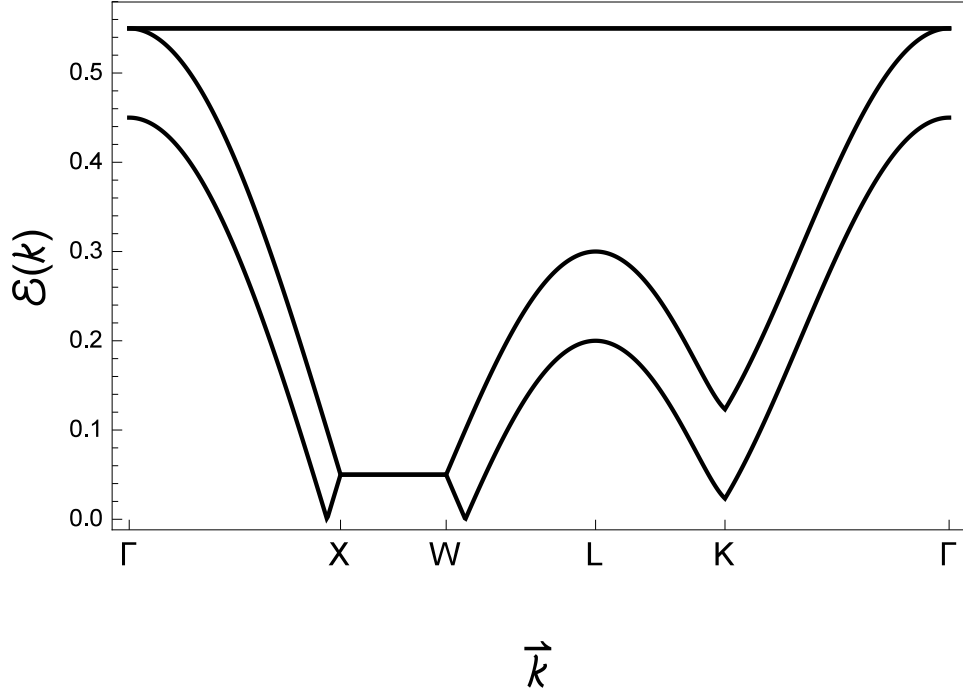


Figure 4.2: Zero-field magnon dispersions for the case when $\tilde{J}_{xx} = J_{yy} = -0.25$ and $\tilde{J}_{zz} = -0.1$. Note that these values are just mathematical and do not correspond to any RE pyrochlore material.

$$Z = \begin{pmatrix} X_R & 0 \\ 0 & X_R \end{pmatrix}, \quad (4.31)$$

where X_R is a 4×4 matrix that contains the orthonormalized eigenvectors of R . One can easily verify that the above formula of Z satisfies the conditions in Eqs. (4.2) and (4.4), i.e. it is the true Bogoliubov matrix. This is the simplest possible form of Z , however, we are not aware of any RE pyrochlore with this constraint on the exchange parameters. In the next section we will treat the most general case within the LSWA.

4.1.3 The General Case

Following Eq. (4.10), we can simplify the eigenvalue equation in terms of a matrix R in the form

$$|R^2 - aR + b\mathbb{1}| = |R - \alpha_+\mathbb{1}| |R - \alpha_-\mathbb{1}| = 0, \quad (4.32)$$

where

$$\alpha_{\pm} = \frac{a}{2} \pm \sqrt{\left(\frac{a^2}{4} - b\right)}, \quad (4.33)$$

and

$$a = \frac{3\tilde{J}_{zz}(\tilde{J}_{xx} + J_{yy})}{\tilde{J}_{xx}J_{yy}}, \quad b = \frac{(9\tilde{J}_{zz}^2 - \varepsilon^2)}{\tilde{J}_{xx}J_{yy}}. \quad (4.34)$$

Consequently, if r is an eigenvalue of R , then one can easily do some algebra with the use of the above equations to get the following relation for the energy dispersions

$$\varepsilon(\vec{k}) = \sqrt{9\tilde{J}_{zz}^2 - \tilde{J}_{xx}J_{yy}r(a - r)}. \quad (4.35)$$

Now, using the eigenvalues of R in Eq. (C.2) (see Appendix C), we find that the general LSWA magnon Hamiltonian has a doubly degenerate flat band which is

$$\varepsilon_{1,2}(\vec{k}) = \sqrt{(3\tilde{J}_{zz} + \tilde{J}_{xx})(3\tilde{J}_{zz} + J_{yy})}, \quad (4.36)$$

and two dispersive bands of the form

$$\varepsilon_{3,4}(\vec{k}) = \sqrt{9\tilde{J}_{zz}^2 - r_{\pm} \left(3\tilde{J}_{zz}(\tilde{J}_{xx} + J_{yy}) - \tilde{J}_{xx}J_{yy}r_{\pm} \right)}. \quad (4.37)$$

Thus, the four energy bands for the AIAO state at zero magnetic field are analytically known and written in the above compact form. A perfect example of RE pyrochlores that fall in this category is $\text{Nd}_2\text{Zr}_2\text{O}_7$ as shown very recently in [43, 44], where the exchange parameters and the values of the g -tensor are listed in Table 3.1. The plot of the energy dispersions for the latest sets of exchange parameters are given in Figure 4.3. We have also plotted the energy dispersions at $\vec{B} = \vec{0}$ through different symmetry directions in Figure 4.4, to compare our results with the results obtained in Ref. [43], see Figure 4.5. Our analytic results agree with the findings in Ref. [43] as can be seen by comparing the vertical axis, the positions where the bands touch, and the curvature of the bands.

Now, we proceed to find the Bogoliubov matrix Z for this general case. First, as we have done in Section 4.1.1, we start with the matrix equation

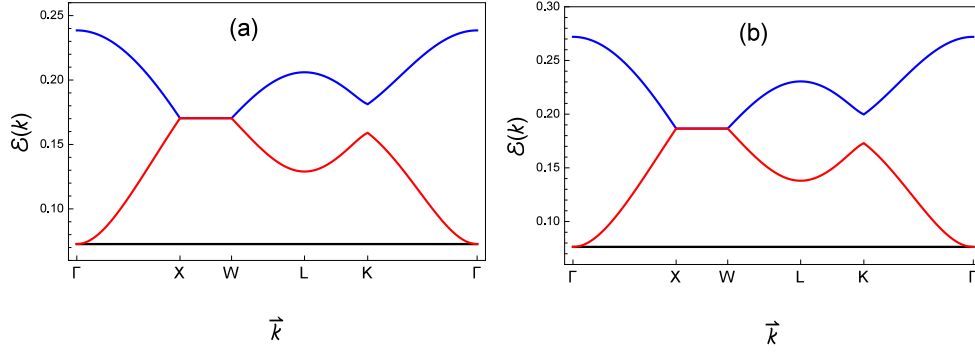


Figure 4.3: Plot of the zero-field energy dispersions of $\text{Nd}_2\text{Zr}_2\text{O}_7$. (a) Using the exchange parameters from [44] and (b) using the corresponding coupling constants from Ref. [43].

$$\mathcal{U}gM\mathcal{U}^\dagger = \begin{pmatrix} 0 & -J_y R + 3\tilde{J}_{zz}\mathbb{1} \\ -\tilde{J}_{xx}R + 3\tilde{J}_{zz}\mathbb{1} & 0 \end{pmatrix}. \quad (4.38)$$

If $\vec{X} = (\vec{u}, \vec{v})^T$ is an eigenvector of $\mathcal{U}gM\mathcal{U}^\dagger$, with little algebra we find

$$\vec{X} = \frac{1}{\sqrt{1 + \left(\frac{-\tilde{J}_{xx}r_i + 3\tilde{J}_{zz}}{\varepsilon_i}\right)^2}} \begin{pmatrix} \vec{u}_i \\ \frac{-\tilde{J}_{xx}r_i + 3\tilde{J}_{zz}}{\varepsilon_i} \vec{u}_i \end{pmatrix}, \quad (4.39)$$

where \vec{u}_i is the orthonormalized eigenvector of R with an eigenvalue r_i . As a result, we find the normalized eigenvector of $\mathcal{G}M$ to be

$$\vec{X} = \frac{1}{\sqrt{2 + 2\left(\frac{-\tilde{J}_{xx}r_i + 3\tilde{J}_{zz}}{\varepsilon_i}\right)^2}} \begin{pmatrix} \left(1 - \frac{-\tilde{J}_{xx}r_i + 3\tilde{J}_{zz}}{\varepsilon_i}\right) \vec{u}_i \\ \left(1 + \frac{-\tilde{J}_{xx}r_i + 3\tilde{J}_{zz}}{\varepsilon_i}\right) \vec{u}_i \end{pmatrix}. \quad (4.40)$$

On the other hand, we follow the procedure in Section 4.1.1 and find that the W_i blocks are

$$W_1 = -\frac{1}{2} \left[\frac{3\tilde{J}_{zz} - \tilde{J}_{xx}r_1}{\varepsilon_1} + \frac{\varepsilon_1}{3\tilde{J}_{zz} - \tilde{J}_{xx}r_1} \right] \mathbb{1}, \quad (4.41)$$

$$W_2 = -\frac{1}{2} \left[\frac{3\tilde{J}_{zz} - \tilde{J}_{xx}r_3}{\varepsilon_3} + \frac{\varepsilon_3}{3\tilde{J}_{zz} - \tilde{J}_{xx}r_3} \right], \quad (4.42)$$

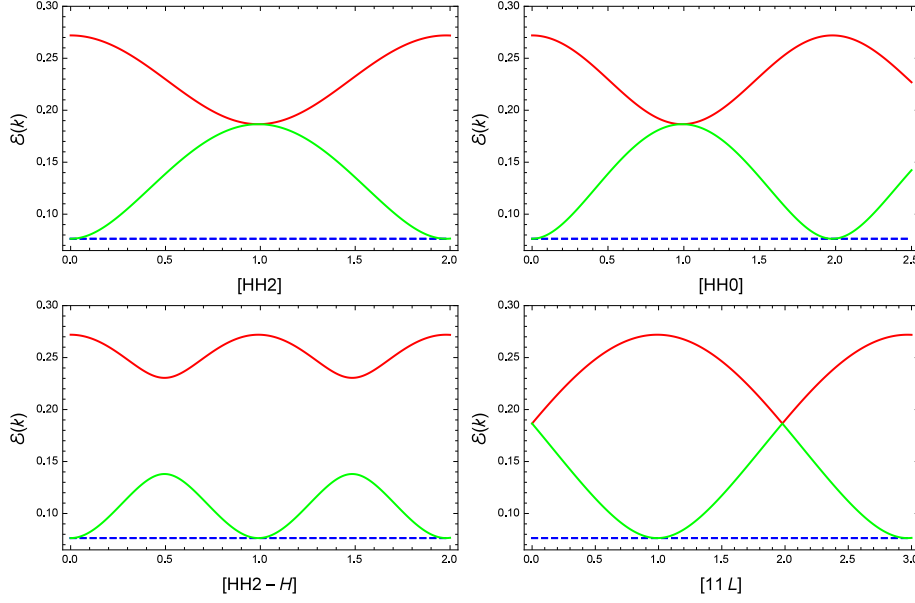


Figure 4.4: Plots of the exact energy dispersions at zero magnetic field for $\text{Nd}_2\text{Zr}_2\text{O}_7$ using the parameters extracted from Ref. [43]. These results show good agreement with the other findings as shown in Figure 4.5.

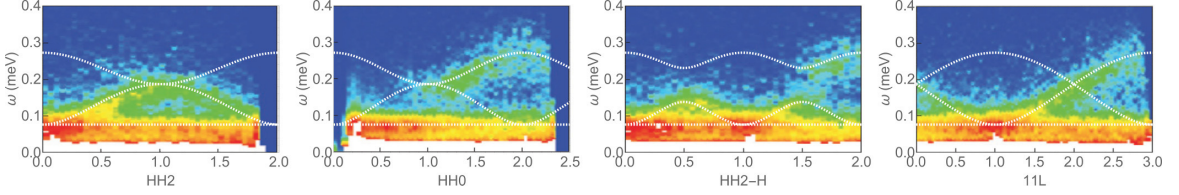


Figure 4.5: Magnon dispersions at zero magnetic field in $\text{Nd}_2\text{Zr}_2\text{O}_7$ found using the inelastic neutron scattering (background) [22] and the calculated energy dispersions (dashed curves) [43]. This picture was taken from [43] with permission. Copyright by the American Physical Society.

$$W_3 = -\frac{1}{2} \left[\frac{3\tilde{J}_{zz} - \tilde{J}_{xx}r_4}{\varepsilon_4} + \frac{\varepsilon_4}{3\tilde{J}_{zz} - \tilde{J}_{xx}r_4} \right]. \quad (4.43)$$

The other three blocks are found by symmetry, i.e. replacing ε_i with $-\varepsilon_i$, giving

$$W_4 = \frac{1}{2} \left[\frac{3\tilde{J}_{zz} - \tilde{J}_{xx}r_1}{\varepsilon_1} + \frac{\varepsilon_1}{3\tilde{J}_{zz} - \tilde{J}_{xx}r_1} \right] \mathbb{1}, \quad (4.44)$$

$$W_5 = \frac{1}{2} \left[\frac{3\tilde{J}_{zz} - \tilde{J}_{xx}r_3}{\varepsilon_3} + \frac{\varepsilon_3}{3\tilde{J}_{zz} - \tilde{J}_{xx}r_3} \right], \quad (4.45)$$

$$W_6 = \frac{1}{2} \left[\frac{3\tilde{J}_{zz} - \tilde{J}_{xx}r_4}{\varepsilon_4} + \frac{\varepsilon_4}{3\tilde{J}_{zz} - \tilde{J}_{xx}r_4} \right]. \quad (4.46)$$

Consequently, using Eq. (4.27) we find the matrix P and thus the full Bogoliubov matrix Z for this general case. This means that we now have the exact results of energy dispersions and normal modes of the RE pyrochlore $\text{Nd}_2\text{Zr}_2\text{O}_7$ [43, 44]. This also covers any RE pyrochlore material that has the same magnetic ordering and follows the symmetry of the $\Gamma_{5,6}$ ground state doublet. Therefore, we have constructed the exact diagonalization of the magnon Hamiltonian for the AIAO state in the $\Gamma_{5,6}$ class of ground state doublet within the LSWA.

4.1.4 $\text{Nd}_2\text{Zr}_2\text{O}_7$ in the [111] Magnetic Field

In the presence of magnetic field along the [111] cubic direction, the effective NN Hamiltonian for the RE ion is given below

$$\mathcal{H}_{\text{eff}}^{\Gamma_{5,6}} = \tilde{\mathcal{H}}^0 + \sum_k L_k^\dagger M(k) L_k, \quad (4.47)$$

where

$$M(k) = \begin{pmatrix} A(k) & B(k) \\ B(k) & A(k) \end{pmatrix}, \quad (4.48)$$

with $A(k)$ defined in Eqs. (3.24-3.28), and $B(k) = \left(\frac{\tilde{J}_{xx} - \tilde{J}_{yy}}{2} \right) R(k)$. As mentioned previously, the energy dispersions $\{\varepsilon_i(\vec{k})\}_{i=1}^4$ are found by calculating the eigenvalues $\{\lambda_i(\vec{k})\}_{i=1}^4$ of the 4×4 matrix $C = A^2 - B^2$, where $\lambda_i(\vec{k}) = \varepsilon_i^2(\vec{k})$. In principle, the eigenvalue equation $|C - \lambda_i(\vec{k})| = 0$ results in a quartic equation in $\lambda_i(\vec{k})$ which has analytic solutions (see Appendix D). Consequently, the energy dispersions are known analytically. As an illustration, we plotted the energy dispersions at different values of the magnetic field in Figure 4.6 in the AIAO state without considering any possible canting of the spins due to the field. We have also added a plot of the energy dispersions of magnons taken from [43] (see Figure 4.7). The latter figure has slight difference from ours due to the canting angle that was considered in the same reference but its value wasn't mentioned in the original article [43].

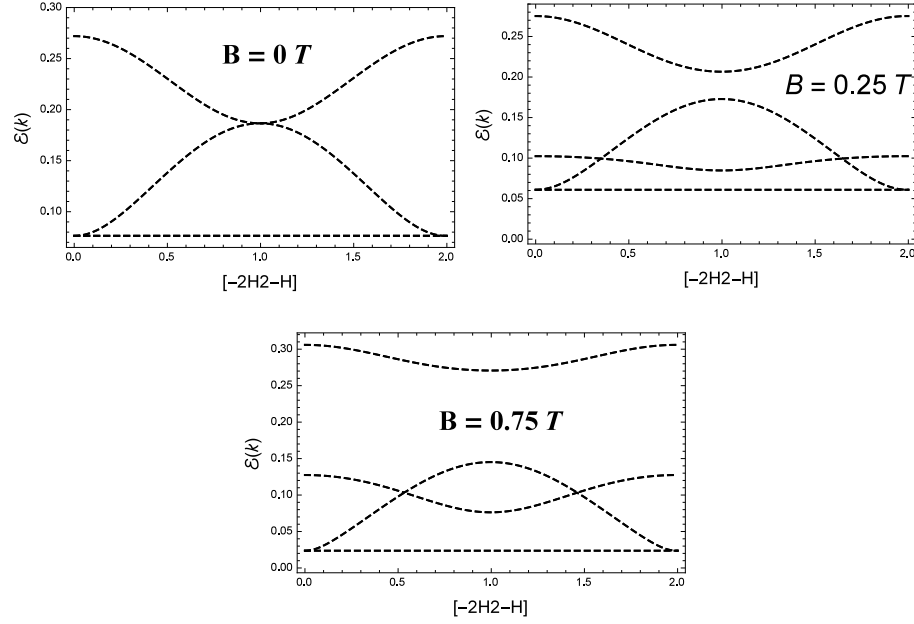


Figure 4.6: Plots of the exact energy dispersions for $\text{Nd}_2\text{Zr}_2\text{O}_7$ in the $[111]$ magnetic field using the parameters from Ref. [43] with zero canting angle.

4.2 Magnon Dispersion in $\text{Er}_2\text{Ti}_2\text{O}_7$ With Antiferromagnetic ψ_2 State

Starting with the effective magnon Hamiltonian Eq. (3.35) in the antiferromagnetic state (ψ_2) of $\text{Er}_2\text{Ti}_2\text{O}_7$, together with Eq. (4.6), we find that the analytic dispersions are given in Eq. (D.7) with the functions $\{S(k), P(k), Q(k)\}$ as defined in Appendix D. However, unlike the $\Gamma_{5,6}$ case, one should rely on numerical methods to find the Bogoliubov matrix $Z(k)$ as discussed in Appendix E. In the case of zero magnetic field, the spins are all pointing along the local x , in this case the exact energy dispersions are plotted in Figure 4.8 where our result agrees with what was obtained in other studies [19?]. Note that when $\vec{B} = 0$, our results show the appearance of soft modes in the energy spectrum, which agrees with the spectral data of $\text{Er}_2\text{Ti}_2\text{O}_7$ where these modes are also signature of the order-by-disorder mechanism observed in this material [19, 39]. We have also calculated the energy dispersions in the case of magnetic field applied along $[1\bar{1}0]$ as shown in Figure 4.9. On the other hand, Ref. [25] have found the energy dispersions in the presence of $[1\bar{1}0]$ and $[111]$ fields (see Figure 4.10), where Figure 4.10 represents a plot of the relative intensities of the spin waves which is

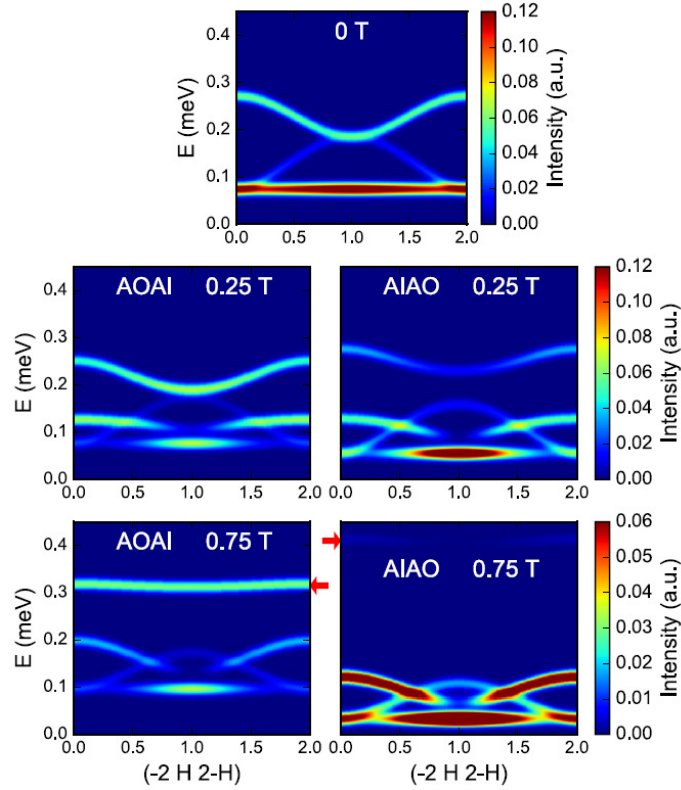


Figure 4.7: Plots of the neutron-scattering spectra for $\text{Nd}_2\text{Zr}_2\text{O}_7$ in the $[111]$ magnetic field for the AIAO and the AOAI (all out-all in) states using the parameters from Ref. [43]. The red arrows at the bottom figures indicate the location of the quasi-flat bands. The whole figure was taken from [43] with permission. Copyright by the American Physical Society.

slightly different from the ordinary plots of the energy dispersions given in this work [25]. A plot of these intensity functions will require the knowledge of the Bogoliubov coefficients and its not within the scope of this work. On the other hand, the difference between our results and the other findings in Ref. [25] is due to the spin polarization where in our work we considered all of the spins aligned with the applied field. It is not clear for us what spin orientations have been considered in Ref. [25] which concludes the sensitivity of the energy dispersions to the spin orientations.

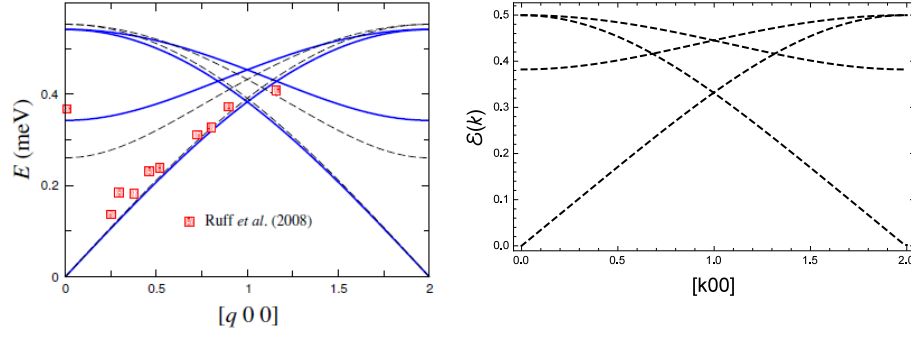


Figure 4.8: Plots of the zero-field energy dispersions for $\text{Er}_2\text{Ti}_2\text{O}_7$. The figure on the left is taken from previous work with permission [19]. We have considered the exchange parameters from Table 3.2. The figure on the right represents our results which matches the previous ones. Copyright by the American Physical Society.

4.3 Exact Dispersions of Magnons for the Ferromagnetic State in $\text{Yb}_2\text{Ti}_2\text{O}_7$

In this section, we will follow the same procedure as in the previous section to plot the exact energy dispersions of magnons in $\text{Yb}_2\text{Ti}_2\text{O}_7$ for the FM state with all of the spins aligned with the external magnetic field applied along the $[1\bar{1}0]$ crystallographic direction. Using the quadratic magnonic Hamiltonian given in Eq. (3.45) and following the diagonalization method introduced in the beginning of this chapter, we plot the associated values of $\{\varepsilon^2(k), \varepsilon(k)\}$ for different values of the magnetic field along different symmetry directions in the Brillouin zone with the exchange constants taken from [36]. In our model, we observe that for low magnetic fields, we get negative values in the $\varepsilon^2(k)$ curves which indicates that magnons are unstable or that our model may not be applicable at low fields (see Figure 4.11). This result is also consistent with the findings in Ref. [36] as the sharp magnon excitations appear at high fields. On the other hand, for $B \geq 2T$, we only observe positive values of $\varepsilon^2(k)$. We also plotted the energy dispersions of magnons for magnetic field strengths $2T$ and $5T$ as shown in Figures 4.12, 4.13, and 4.14. For instance, if we compare our analytic results in Figure 4.13 vs the numerical results found in Figure 4.15 we find a good agreement between both figures for the energy dispersions plotted through several symmetry directions in the presence of $5T$ field [36] which is obvious by looking at the features of the spectrum such as the appearance of quasi-flat band [36] (slightly above 1.4 meV), energy bands crossing, and the curvature of the bands through the given symmetry

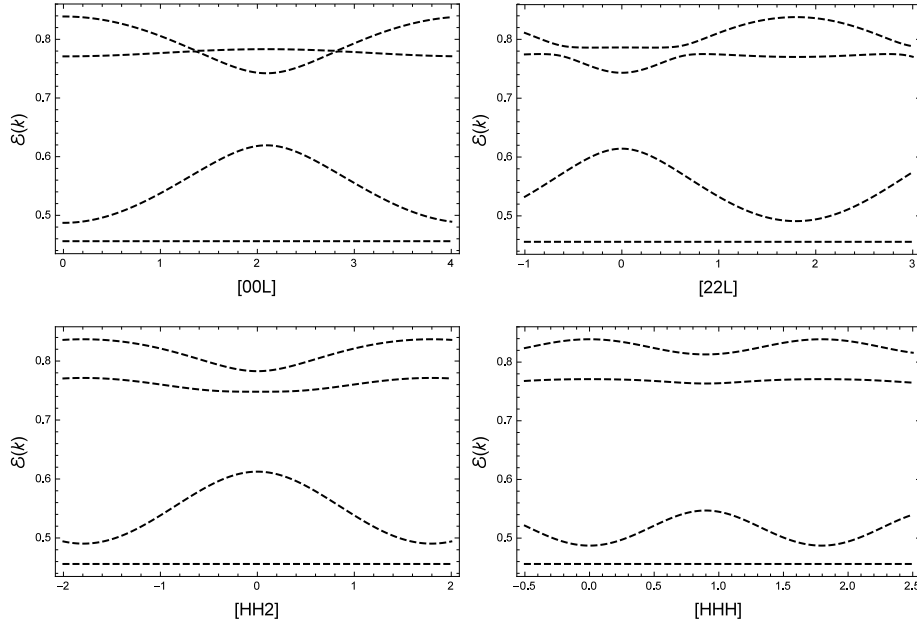


Figure 4.9: Plot of the exact dispersions of magnons in $\text{Er}_2\text{Ti}_2\text{O}_7$ for magnetic field of strength $3T$ applied along $[1\bar{1}0]$ using the exchange parameters from Table 3.2. The spins are considered to be fully polarized with the applied field.

directions.

On the other hand, we plotted magnon dispersions when $B = 2T$ in Figure 4.12. A plot of the spin wave intensities for this case is given in Figure 4.16 which was adopted from Ref. [36]. Now, by looking at the vertical axes of both figures we can tell there are similarities especially the appearance of the top band around 1 meV, but both figures are still different in the sense that they represent different quantities. Furthermore, we have reevaluated the energy dispersions for the same case (the field applied along the $[1\bar{1}0]$ and the spins aligned with the field) using the fitting parameters from Ref. [5] as shown in Figure 4.14, see Table 3.3 for the values of the exchange parameters in both cases. Comparing Figures 4.12 and Figure 4.13 with Figure 4.14, we find differences in each case which is due to the sensitivity of the energy dispersion to the fitting parameters. However, the three figures still share the same features in the spectrum such as the appearance of the quasi-flat bands at $5T$ field for both sets of exchange parameters taken from references [36] and [5] (see Table 3.3). This also raises a question on the dependence of the extracted exchange parameters on the canting angle in different fields.

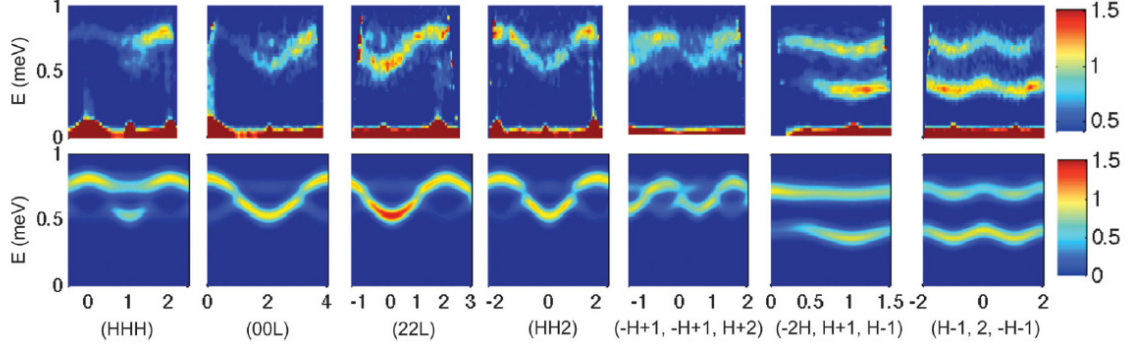


Figure 4.10: Neutron scattering measurements of the spin wave excitations (top row) and calculated (bottom row) dispersions of magnons in $\text{Er}_2\text{Ti}_2\text{O}_7$ for magnetic field of strength $3T$. For the first five columns, the magnetic field was taken along the $[1\bar{1}0]$ and for the rest \vec{B} is aligned with the $[111]$ direction. The whole figure was taken from Ref. [25] with permission. Copyright by the American Physical Society.

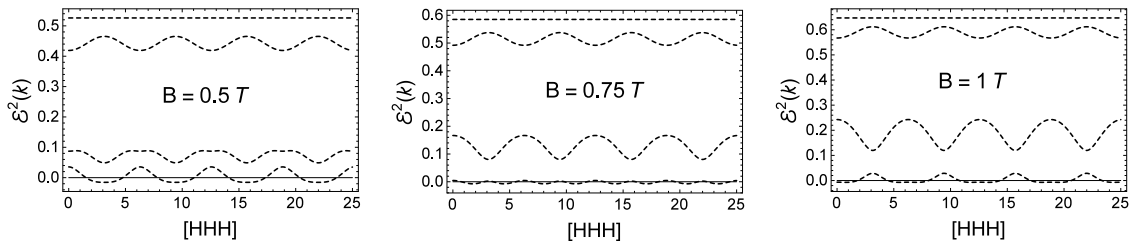


Figure 4.11: Low field plots of $\varepsilon^2(\vec{k})$ for $\text{Yb}_2\text{Ti}_2\text{O}_7$ with an external magnetic field (B) applied parallel to the $[1, \bar{1}, 0]$ for different field strengths as indicated in the legends. The exchange parameters and the g -tensor were taken from Ref. [36](see Table 3.3).

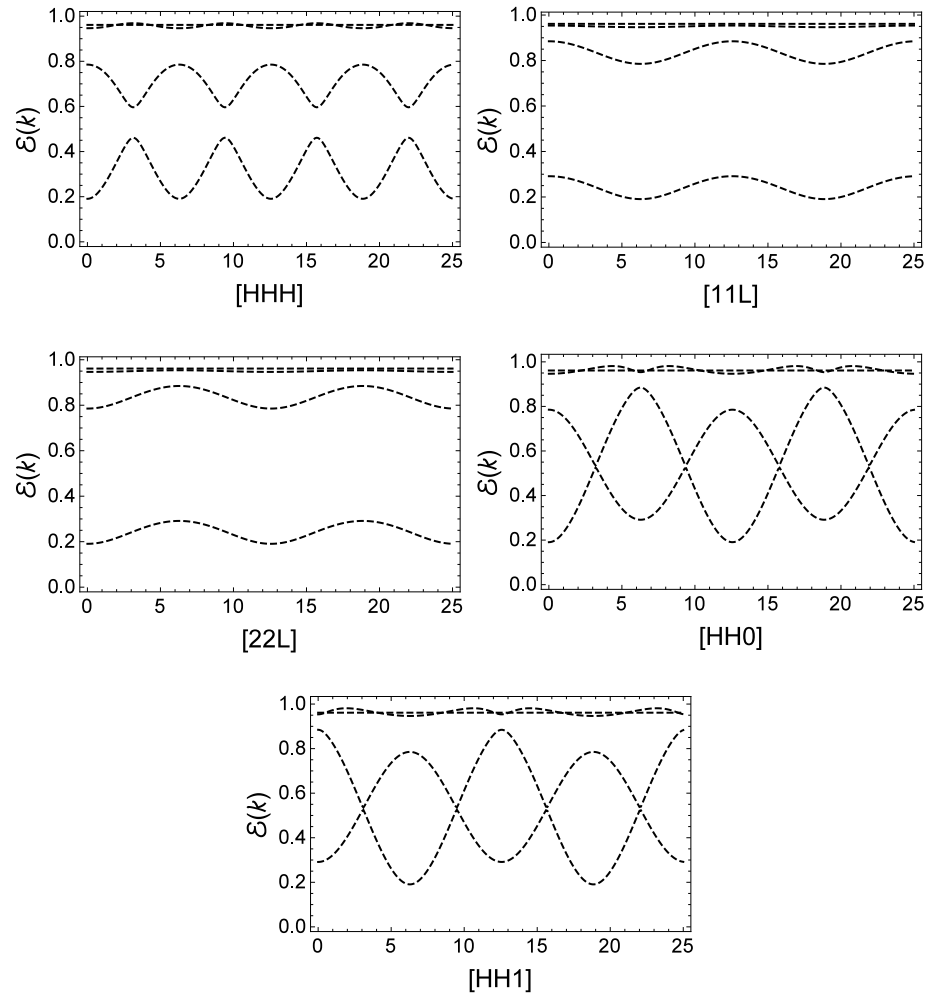


Figure 4.12: Magnon dispersions in $\text{Yb}_2\text{Ti}_2\text{O}_7$ with an applied magnetic field of strength $2T$ along the $[1, \bar{1}, 0]$ direction. The exchange parameters and the g -tensor were taken from Ref. [36] for the sake of comparison.

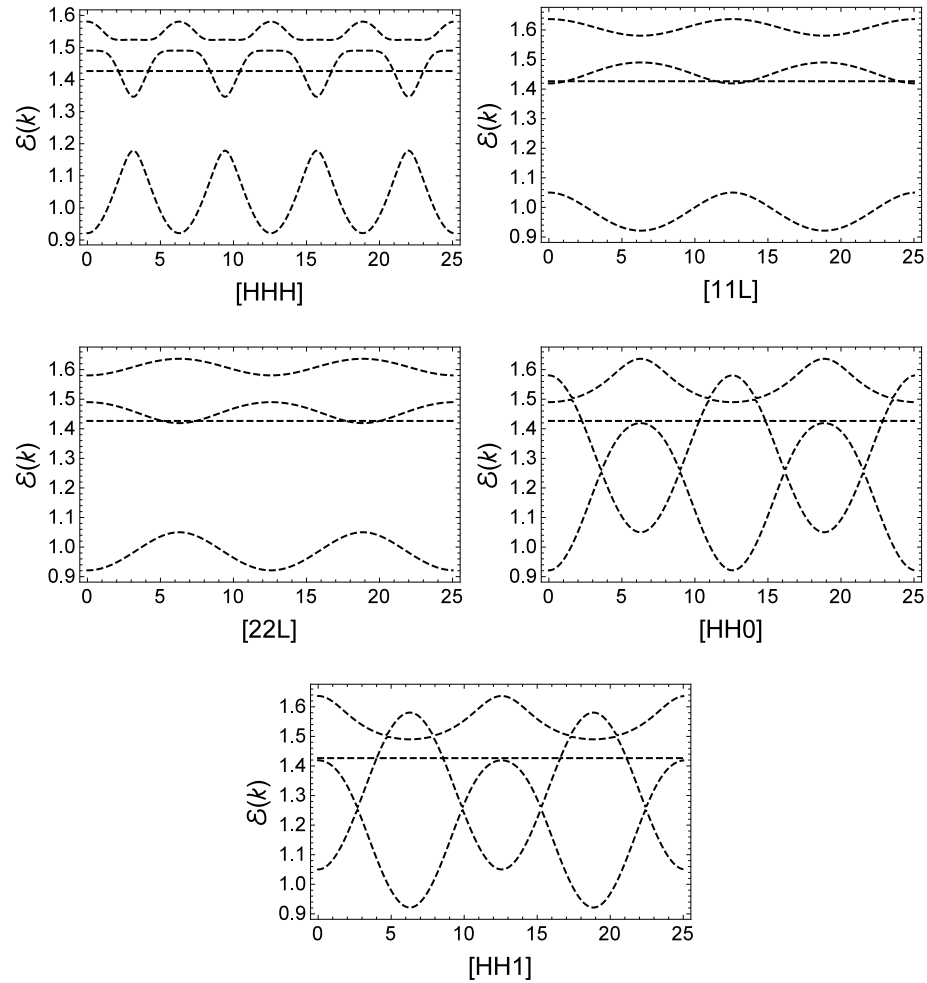


Figure 4.13: Magnon dispersions in $\text{Yb}_2\text{Ti}_2\text{O}_7$ with an applied magnetic field of strength $5T$ along the $[1, \bar{1}, 0]$ direction. The exchange parameters and the g -tensor were taken from Ref. [36] for the sake of comparison, see Table 3.3 for more details.

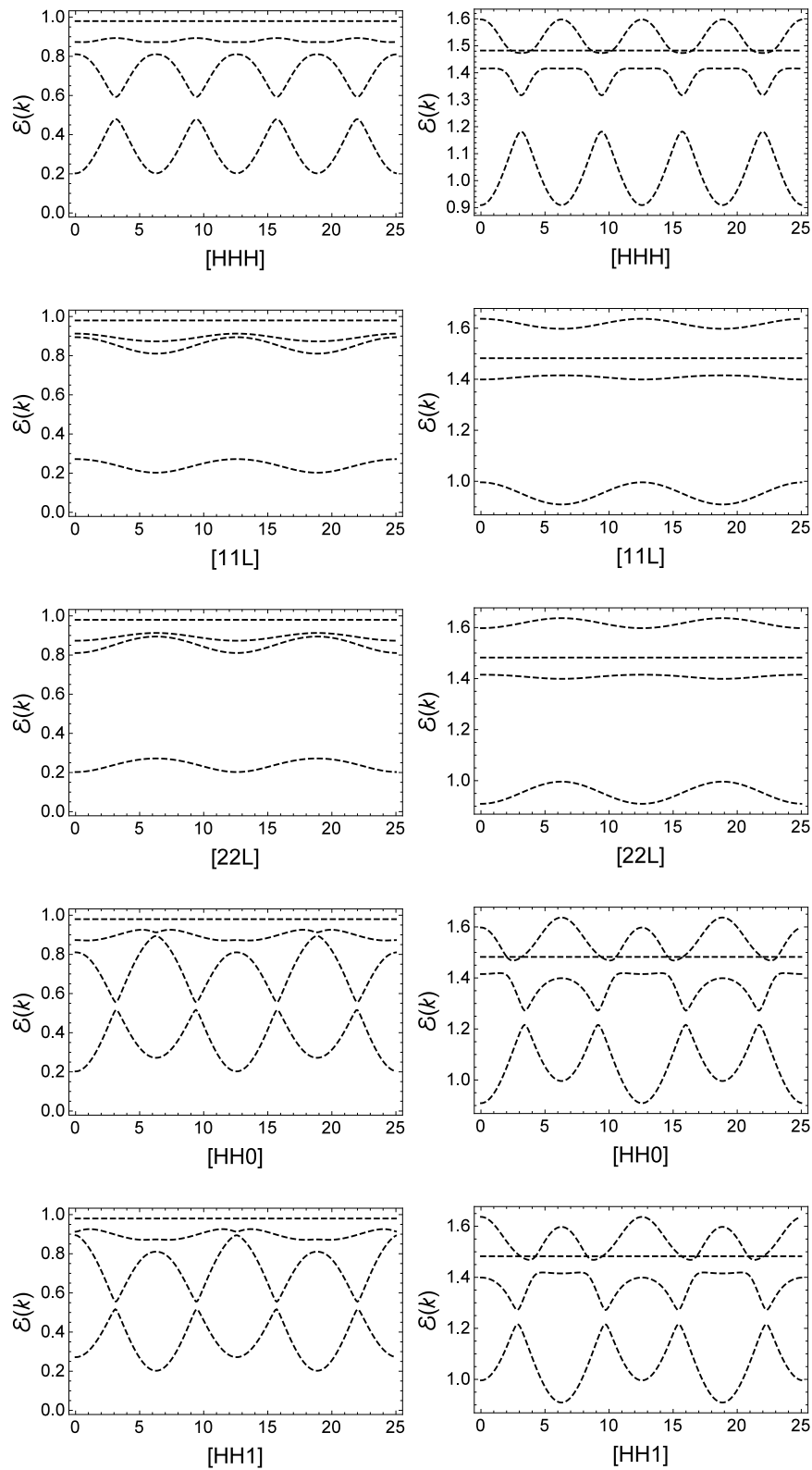


Figure 4.14: Magnon dispersions in $\text{Yb}_2\text{Ti}_2\text{O}_7$ with an applied magnetic field of strengths $5T$ (right column) and $2T$ (left column) along the $[1, \bar{1}, 0]$ direction. The exchange parameters and the g -tensor were taken from Ref. [5] (see Table 3.3) for the sake of comparison with the dispersions obtained using the parameters from Ref. [36].

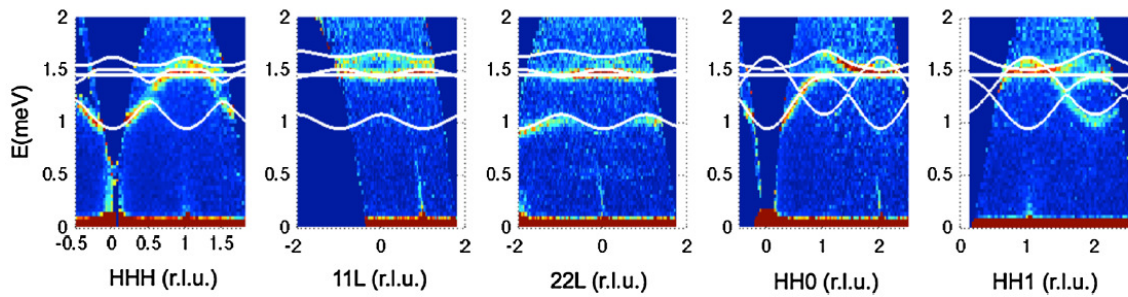


Figure 4.15: Energy dispersions of magnons in $\text{Yb}_2\text{Ti}_2\text{O}_7$ with an applied magnetic field of strength $5T$ parallel to $[1, \bar{1}, 0]$. The white curves represent LSWA fitting over the experimental dispersions. This figure was taken from Ref. [36] with permission. Copyright by the American Physical Society.

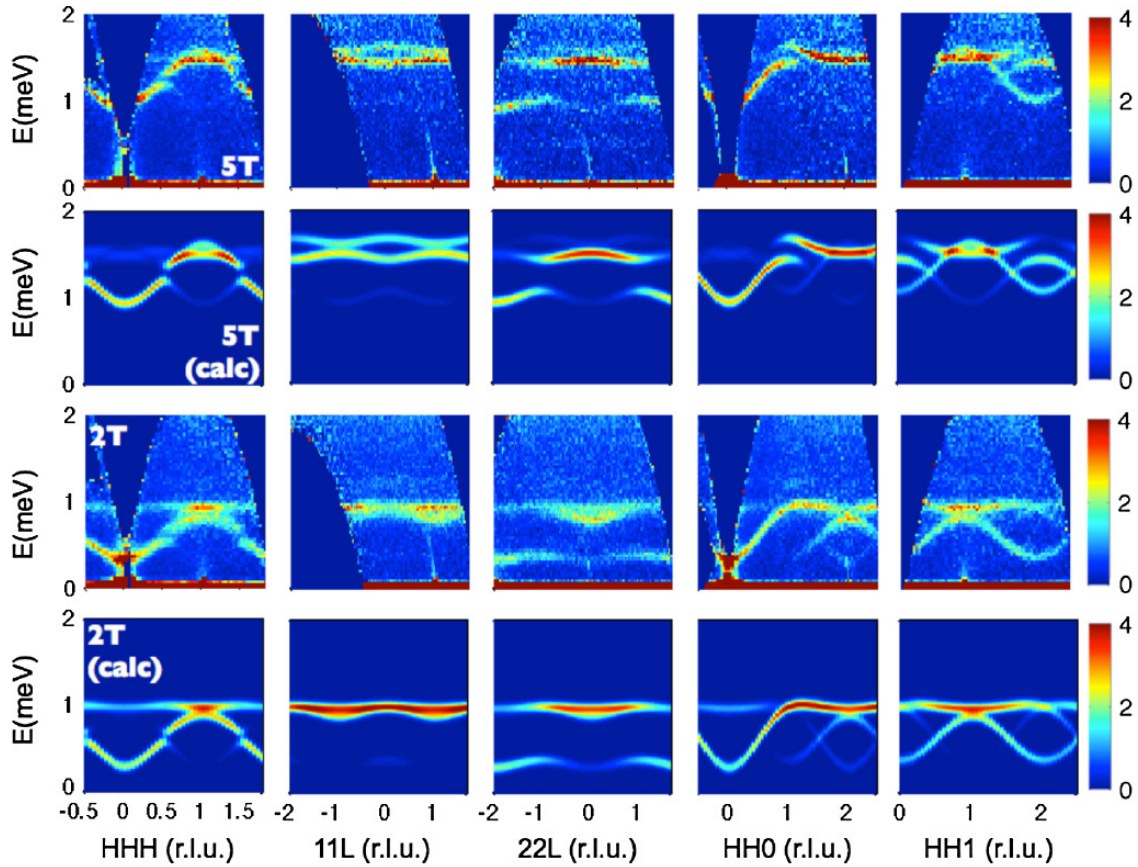


Figure 4.16: Plots of the measured and calculated (calc) spin wave dispersions in $\text{Yb}_2\text{Ti}_2\text{O}_7$ for magnetic field applied along the $[1, \bar{1}, 0]$ direction. The first two rows are for the measured and the calculated dispersions at 5 T field, respectively. The lower two rows represent the experimental and computed magnon dispersions for the magnetic field with strength 2T, respectively. Note that r.l.u. stands for reciprocal lattice unit. This figure was taken from [36] with permission. Copyright by the American Physical Society.

4.4 Summary

We would like to summarize our results as follows. For the $\Gamma_{5,6}$ GSD, we considered the AIAO ordered state. We present the exact analytic diagonalization of the magnon Hamiltonian within the LSWA. This applies perfectly to $\text{Nd}_2\text{Zr}_2\text{O}_7$. For the Γ_4 case, we found the exact energy dispersions of magnons in $\text{Er}_2\text{Ti}_2\text{O}_7$ and $\text{Yb}_2\text{Ti}_2\text{O}_7$ in their AFM and FM states, respectively. However, the Bogoliubov matrix $Z(k)$ is not found analytically, as explained in Sections 4.2 and 4.3. In the next chapter we give our conclusions and future directions.

Chapter 5

Conclusions and Future Directions

In this work we have studied a special class of rare-earth pyrochlores in which the RE ions have a crystal electric field ground state doublet that is separated from the first excited state by approximately 100 K or more. These materials are then considered as effective spin-1/2 systems which is why they are called quantum rare-earth pyrochlores. Based on symmetry, the CEF ground state doublet comes into three different varieties labeled as Γ_3 , Γ_4 , and $\Gamma_{5,6}$. For each of these doublets, the exchange interactions are generally represented in terms of pseudo-spin operators and have slightly different forms depending on the type of doublet. Only in one of these doublets, the Γ_4 doublet are the spin operators isomorphic to real spin-1/2 operators, and so they transform the same way as physical spinors under space operations and time reversal. However, the pseudo-spins in the other doublets transform differently as summarized in Table 2.1. We have considered several examples of QREPs that belong to $\{\Gamma_4, \Gamma_{5,6}\}$ doublets for which we have the experimental values of the exchange parameters for only few of those materials. For the Γ_3 doublet, we are not aware of any example with known values of the exchange parameters; this doublet has the same linear spin wave analysis as the Γ_4 doublet, except that $J_{2\pm} = 0$.

For the $\Gamma_{5,6}$ doublet, we have considered an all in-all out ordered state and we have done the linear spin wave analysis at zero magnetic field and found the exact energy dispersions $\{\varepsilon(\vec{k})_i\}_{i=1}^4$ and the associated Bogoliubov matrix $Z(k)$ for different cases including the general case. This applies perfectly for the RE pyrochlore $\text{Nd}_2\text{Zr}_2\text{O}_7$ which orders in the AIAO state near 0.285 K [22, 23, 43, 44]. The results obtained for

this case might also be applied to another RE pyrochlore which is $\text{Sm}_2\text{Ti}_2\text{O}_7$ (see Ref. [24] for more details on this material). On the other hand, these results will be very useful for further investigation on the limitations of the LSWA in $\text{Nd}_2\text{Zr}_2\text{O}_7$ when studying different physical quantities or thermodynamic properties which is something of interest for us.

In the Γ_4 GSD, we have investigated the magnon dispersions for $\text{Er}_2\text{Ti}_2\text{O}_7$ and $\text{Yb}_2\text{Ti}_2\text{O}_7$. The rare-earth pyrochlore $\text{Er}_2\text{Ti}_2\text{O}_7$ orders antiferromagnetically in the ψ_2 state (all of the spins are pointing along the local x at each site) near 1.2 K. In our calculations of the exact energy dispersions which are given in Eq. D.7, we have considered magnetic fields along the $[111]$ and $[1\bar{1}0]$ directions. At zero magnetic field, the spectrum shows the appearance of soft modes which agrees with the previous results on this material. However, at slightly higher fields, our model shows the appearance of negative values of some of the $\varepsilon_i^2(\vec{k})$ curves which indicates the limitations of our NN and LSWA approximations. On the other hand, at high fields we don't face this problem and all the curves in $\varepsilon_i^2(\vec{k})$ are positive. In addition to $\text{Er}_2\text{Ti}_2\text{O}_7$, we studied magnons in $\text{Yb}_2\text{Ti}_2\text{O}_7$ which orders in a FM state near 0.2 K. In the latter material we considered magnetic fields along the $[1\bar{1}0]$ cubic direction with spins aligned with the applied field. Similar to $\text{Er}_2\text{Ti}_2\text{O}_7$, we found that the low fields parts of the $\varepsilon_i^2(\vec{k})$ curves have some negative values along different symmetry directions. At higher fields we always get positive values in the $\varepsilon_i^2(\vec{k})$ plots along the given symmetry paths. We plotted the associated exact energy dispersions for both materials at different values of the magnetic fields. Unlike the energy dispersions, exact analytic calculations of Bogoliubov matrix is not possible for those two cases and one has to rely on numerical methods following the procedure in Appendix E. Very recently, Thompson *et al.* [5] showed that $\text{Yb}_2\text{Ti}_2\text{O}_7$ has strong quantum fluctuations at low temperature which requires more care in doing the spin wave calculations as some higher order magnon-magnon interaction terms may be necessary for a better description of magnons in this material.

Finally, in summary of our work, we have obtained the exact analytic energy dispersions of magnons for three materials $\text{Nd}_2\text{Zr}_2\text{O}_7$, $\text{Er}_2\text{Ti}_2\text{O}_7$, and $\text{Yb}_2\text{Ti}_2\text{O}_7$. Our analytic results have been tested against the numerical findings that have been obtained in previous studies and showed good agreement. On top of that, we were able

to calculate the exact analytic form of the Bogoliubov matrix Z for the zero-field AIAO state of the $\Gamma_{5,6}$ doublet. Consequently, within the LSWT, exact diagonalization of the magnonic Hamiltonian for $\text{Nd}_2\text{Zr}_2\text{O}_7$ has been obtained. This latter result, up to our knowledge, have not been obtained in the literature before [22, 23, 43, 44]. However, numerical calculations magnon dispersions in $\text{Er}_2\text{Ti}_2\text{O}_7$, and $\text{Yb}_2\text{Ti}_2\text{O}_7$ have been published before and we have reproduced the results and obtain also our analytic calculations of these dispersions and we found good agreement [25, 36]. For future work, we would like to consider modeling the magnon-magnon interactions to improve modeling the magnonic Hamiltonian for these effective pseudo-spin 1/2 systems. We would like also to apply our results to other rare-earth pyrochlore systems that with a CEF ground state doublet.

Bibliography

- [1] Curnoe, S. H. Quantum spin configurations in $\text{Tb}_2\text{Ti}_2\text{O}_7$. *Physical Review B*, 75(21):212404, 2007.
- [2] Gardner, J. S., *et al.* Dynamic frustrated magnetism in $\text{Tb}_2\text{Ti}_2\text{O}_7$ at 50mK. *Physical Review B*, 68(18):180401, 2003.
- [3] Gingras, M. J. P., *et al.* Thermodynamic and single-ion properties of Tb^{+3} within the collective paramagnetic-spin liquid state of the frustrated pyrochlore antiferromagnet $\text{Tb}_2\text{Ti}_2\text{O}_7$. *Physical Review B*, 62(10):6496, 2000.
- [4] Gardner, J. S., *et al.* Neutron scattering studies of the cooperative paramagnet pyrochlore $\text{Tb}_2\text{Ti}_2\text{O}_7$. *Physical Review B*, 64(22):224416., 2001.
- [5] Thompson, J. D., McClarty, P. A., Prabhakaran, D., Cabrera, I., Guidi, T., Coldea, R. Quasiparticle breakdown and spin hamiltonian of the frustrated quantum pyrochlore $\text{Yb}_2\text{Ti}_2\text{O}_7$ in a magnetic field. *Physical Review Letters*, 119(5):057203, 2017.
- [6] Castelnovo, C., Moessner, R., Sondhi, S. L. Magnetic monopoles in spin ice. *Nature*, 451(7174):42, 2008.
- [7] Anderson, P. W . Ordering and antiferromagnetism in ferrites. *Physical Review*, 102(4):1008, 1956.
- [8] Bramwell, S. T., *et al.* Spin correlations in $\text{Ho}_2\text{Ti}_2\text{O}_7$: A dipolar spin ice system. *Physical Review Letters*, 87(4):047205, 2001.
- [9] Harris, M. J., Bramwell, S. T., McMorrow, D. F., Zeiske, T. H., Godfrey, K. W. Geometrical frustration in the ferromagnetic pyrochlore $\text{Ho}_2\text{Ti}_2\text{O}_7$. *Physical Review Letters*, 79(13):2554, 1997.

- [10] Morris, D. J. P., *et al.* Dirac strings and magnetic monopoles in the spin ice $\text{Dy}_2\text{Ti}_2\text{O}_7$. *Science*, 236(5951):411-414, 2009.
- [11] Ramirez, A. P., Hayashi, A., Cava, R. A., Siddharthan, R., Shastry, B. S. Zero point entropy in spin ice. *Nature*, 399(6734):333, 1999.
- [12] Aoki, H., Sakakibara, T., Matsuhira, K., Hiroi, Z. Magnetocaloric effect study on the pyrochlore spin ice compound $\text{Dy}_2\text{Ti}_2\text{O}_7$ in a [111] magnetic field. *Journal of the Physical Society of Japan*, 73(10):2851-2856., 2004.
- [13] Higashinaka, R., Fukazawa, H., Deguchi, K., Maeno, Y. Low temperature specific heat of $\text{Dy}_2\text{Ti}_2\text{O}_7$ in the kagome ice state. *Journal of the Physical Society of Japan*, 73(10):2845-2850., 2004.
- [14] Brooks-Bartlett, M. E., Banks, S. T., Jaubert, L. D., Harman-Clarke, A., Holdsworth, P. C. Magnetic-moment fragmentation and monopole crystallization. *Physical Review X*, 4(1):011007, 2014.
- [15] Gaudet, J., *et al.* Gapless quantum excitations from an icelike splayed ferromagnetic ground state in stoichiometric $\text{Yb}_2\text{Ti}_2\text{O}_7$. *Physical Review B*, 93(6):064406, 2016.
- [16] Peanha-Antonio, V., *et al.* Magnetic excitations in the ground state of $\text{Yb}_2\text{Ti}_2\text{O}_7$. *Physical Review B*, 96(21):214415, 2017.
- [17] Champion, J. D. M., *et al.* $\text{Er}_2\text{Ti}_2\text{O}_7$: Evidence of quantum order by disorder in a frustrated antiferromagnet. *Physical Review B*, 68(2):020401, 2003.
- [18] Ruff, J. P. C., *et al.* Spin waves and quantum criticality in the frustrated XY pyrochlore antiferromagnet $\text{Er}_2\text{Ti}_2\text{O}_7$. *Physical Review Letters*, 101(14):147205, 2008.
- [19] Zhitomirsky, M. E., Gvozdkova, M. V., Holdsworth, P. C. W., Moessner, R. Quantum order by disorder and accidental soft mode in $\text{Er}_2\text{Ti}_2\text{O}_7$. *Physical Review Letters*, 109(7):077204, 2012.
- [20] Yan, H., Benton, O., Jaubert, L., Shannon, N. Theory of multiple-phase competition in pyrochlore magnets with anisotropic exchange with application to $\text{Yb}_2\text{Ti}_2\text{O}_7$, $\text{Er}_2\text{Ti}_2\text{O}_7$, and $\text{Er}_2\text{Sn}_2\text{O}_7$. *Physical Review B*, 95(9):094422, 2017.

- [21] Kittel, C. and Fong, C. Y. *Quantum theory of solids*. New York: Wiley, 1963.
- [22] Petit, S., *et al.* Observation of magnetic fragmentation in spin ice. *Nature Physics*, 12(8):746, 2016.
- [23] Benton, O. Quantum origins of moment fragmentation in $\text{Nd}_2\text{Zr}_2\text{O}_7$. *Physical Review B*, 94(10):104430, 2016.
- [24] Mauws, C., *et al.* Dipolar-octupolar ising antiferromagnetism in $\text{Sm}_2\text{Ti}_2\text{O}_7$. *Physical Review B*, 98(10):100401, 2018.
- [25] Savary, L., Ross, K. A., Gaulin, B. D., Ruff, J. P., Balents, L. Order by quantum disorder in $\text{Er}_2\text{Ti}_2\text{O}_7$. *Physical review letters*, 109(16):167201, 2012.
- [26] Mukherjee, S. P., Curnoe, S. H. Effective spin-1 2 exchange interactions in $\text{Tb}_2\text{Ti}_2\text{O}_7$. *Physical Review B*, 90(21):214404, 2014.
- [27] Tinkham, M. *Group Theory and Quantum Mechanics*. McGraw-Hill Inc., New York, USA, 1964.
- [28] Curnoe, S. H. Exchange interactions in two-state systems: rare earth pyrochlores. *Journal of Physics: Condensed Matter*, 30(23):235803, 2018.
- [29] Zinkin, M. P., Harris, M. J., Tun, Z., Cowley, R. A., Wanklyn, B. M. Lifting of the ground-state degeneracy by crystal-field interactions in the pyrochlore $\text{Tm}_2\text{Ti}_2\text{O}_7$. *Journal of Physics: Condensed Matter*, 8(2):193, 1996.
- [30] Bertin, A., Chapuis, Y., de Rotier, P. D., Yaouanc, A. Crystal electric field in the $\text{R}_2\text{Ti}_2\text{O}_7$ pyrochlore compounds. *Journal of Physics: Condensed Matter*, 24(25):256003., 2012.
- [31] Gardner, J. S., Ehlers, G. Magnetic order and crystal field excitations in $\text{Er}_2\text{Ru}_2\text{O}_7$: a neutron scattering study. *Journal of Physics: Condensed Matter*, 21(43):436004, 2009.
- [32] Mirebeau, I., Bonville, P., Hennion, M. Magnetic excitations in $\text{Tb}_2\text{Sn}_2\text{O}_7$ and $\text{Tb}_2\text{Ti}_2\text{O}_7$ as measured by inelastic neutron scattering. *Physical Review B*, 76(18):184436, 2007.
- [33] Ryabov, I. D. On the generation of operator equivalents and the calculation of their matrix elements. *Journal of Magnetic Resonance*, 140(1):141-145, 1999.

- [34] Griffiths, D. J. *Introduction to quantum mechanics*. Pearson Prentice Hall, New Jersey, USA, 2005.
- [35] Cohen-Tannoudji, C., Diu, B., Lalo, F. *Quantum mechanics*; Mécanique quantique. Walter De Gruyter, Berlin, Germany, 2000.
- [36] Ross, K. A., *et al.* Quantum excitations in quantum spin ice. *Physical Review X*, 1(2):021002, 2011.
- [37] Robert, J., *et al.* Spin dynamics in the presence of competing ferromagnetic and antiferromagnetic correlations in $\text{Yb}_2\text{Ti}_2\text{O}_7$. *Physical Review B*, 92(6):064425., 2015.
- [38] Yaouanc, A., *et al.* Dynamical splayed ferromagnetic ground state in the quantum spin ice $\text{Yb}_2\text{Sn}_2\text{O}_7$. *Physical Review Letters*, 110(12):127207, 2013.
- [39] Rau, J. G., Gingras, M. J. Frustrated quantum rare-earth pyrochlores. *Annual Review of Condensed Matter Physics*, 10:357-386, 2019.
- [40] Holstein, T., Primakoff, H. . Field dependence of the intrinsic domain magnetization of a ferromagnet. *Physical Review*, 58(12):1098., 1940.
- [41] McClarty, P. A., Curnoe, S. H., Gingras, M. J. P. Energetic selection of ordered states in a model of the $\text{Er}_2\text{Ti}_2\text{O}_7$ frustrated pyrochlore XY antiferromagnet. *Journal of Physics: Conference Series*, 145(1):012032, 2009.
- [42] Palmer, S. E., Chalker, J. T. Order induced by dipolar interactions in a geometrically frustrated antiferromagnet. *Physical Review B*, 62(1):488, 2000.
- [43] Xu, J., *et al.* Anisotropic exchange hamiltonian, magnetic phase diagram, and domain inversion of $\text{Nd}_2\text{Zr}_2\text{O}_7$. *Physical Review B*, 99(14):144420, 2019.
- [44] Lhotel, E., *et al.* Evidence for dynamic kagome ice. *Nature communications*, 9(1):3786, 2018.
- [45] Lee, E. K. H., Bhattacharjee, S., Kim, Y. B. Magnetic excitation spectra in pyrochlore iridates. *Physical Review B*, 87(21), 214416, 2013.
- [46] Lee, S., Paramakanti, A., Kim, Y. B. RKKY interactions and the anomalous Hall effect in metallic rare-earth pyrochlores. *Physical review letters*, 111(19), 196601, 2013.

- [47] Del Maestro, Adrian G., and Michel JP Gingras. Quantum spin fluctuations in the dipolar heisenberg-like rare earth pyrochlores. *Journal of Physics: Condensed Matter*, 16(20):3339, 2004.
- [48] Bonville, P.,*et al.* Transitions and spin dynamics at very low temperature in the pyrochlores $\text{Yb}_2\text{Ti}_2\text{O}_7$ and $\text{Gd}_2\text{Sn}_2\text{O}_7$. *Hyperfine interactions*, 156(1-4):103-111, 2004.
- [49] Fennell, T.,*et al.* Magnetic coulomb phase in the spin ice $\text{Ho}_2\text{Ti}_2\text{O}_7$. *Science*, 326(5951):415-417, 2009.
- [50] Hodges, J. A.,*et al.* First-order transition in the spin dynamics of geometrically frustrated $\text{Yb}_2\text{Ti}_2\text{O}_7$. *Physical Review Letters*, 88(7):077204, 2002.

Appendix A

Stevens Operators and the CEF Ground States

First, we begin by listing the six Stevens operators given in \mathcal{H}_{CEF} which take the forms [33]

$$\mathcal{O}_2^0 = 3J_z^2 - J(J+1), \quad (\text{A.1})$$

$$\mathcal{O}_4^0 = 35J_z^4 + (25 - 30J - 30J^2)J_z^2 + 3J(J+1)(J^2 + J - 6), \quad (\text{A.2})$$

$$\mathcal{O}_4^3 = \frac{1}{4}\{J_z, J_+^3 + J_-^3\}, \quad (\text{A.3})$$

$$\begin{aligned} \mathcal{O}_6^0 = & [105J^2(J+1)^2 - 525J(J+1)294] J_z^2 + (753 - 315J - 315J^2)J_z^4 \\ & + 231J_z^6 + 5J^2(J+1)^2(8 - J - J^2), \end{aligned} \quad (\text{A.4})$$

$$\mathcal{O}_6^3 = \frac{1}{4}\{J_+^3 + J_-^3, 11J_z^3 - (59 + 3J + 3J^2)J_z\}, \quad (\text{A.5})$$

$$\mathcal{O}_6^6 = \frac{J_+^6 + J_-^6}{2}, \quad (\text{A.6})$$

where $\{A, B\}$ denotes the anti-commutator of two operators, i.e. $\{A, B\} = AB + BA$. For completeness, we list the ground state doublets for few of the rare earth titanates with interest as in Table A.1 below. Thus, one can easily calculate the ground state energies using the CEF Hamiltonian together with the supplementary data in Table 1.2 and Table A.1.

Table A.1: The GSD of few rare earth titanates $R_2Ti_2O_7$ [24, 30].

R	GSD	Type
Tb	$0.266 \pm 5\rangle \mp 0.133 \pm 2\rangle - 0.129 \mp 1\rangle \mp 0.946 \mp 4\rangle$	Γ_3
Dy	$0.981 \pm \frac{15}{2}\rangle \pm 0.190 \pm \frac{9}{2}\rangle - 0.022 \pm \frac{3}{2}\rangle \mp 0.037 \mp \frac{3}{2}\rangle + 0.005 \mp \frac{9}{2}\rangle \pm 0.001 \mp \frac{15}{2}\rangle$	$\Gamma_{5,6}$
Ho	$-0.979 \pm 8\rangle \pm 0.189 \pm 5\rangle - 0.014 \pm 2\rangle \pm 0.07 \mp 1\rangle - 0.031 \mp 4\rangle \pm 0.005 \mp 7\rangle$	Γ_3
Er	$0.471 \pm \frac{13}{2}\rangle \pm 0.421 \pm \frac{7}{2}\rangle - 0.569 \pm \frac{1}{2}\rangle \mp 0.240 \mp \frac{5}{2}\rangle + 0.469 \mp \frac{11}{2}\rangle$	Γ_4
Yb	$0.376 \pm \frac{7}{2}\rangle + 0.922 \pm \frac{1}{2}\rangle - 0.093 \mp \frac{5}{2}\rangle$	Γ_4
Sm	$ \pm \frac{3}{2}\rangle$	$\Gamma_{5,6}$

Appendix B

The Local Coordinate System

Generally, the CEF measurements consider the local environment of the magnetic RE ion [29, 31, 32]. Thus, it is useful to define a local reference frame in which we perform our theoretical calculations. For convenience, we choose the local \hat{z}_i axis to be parallel to the three-fold axis C_3 at each site. Following Figure 1.2, we labeled the four basis ions with numbers 1 \rightarrow 4 with the following local positions expressed with the respect to the global cubic axes,

$$\hat{x}_1 = \frac{1}{\sqrt{6}}(1, 1, -2), \quad \hat{y}_1 = \frac{1}{\sqrt{2}}(-1, 1, 0), \quad \hat{z}_1 = \frac{1}{\sqrt{3}}(1, 1, 1), \quad (\text{B.1})$$

$$\hat{x}_2 = \frac{1}{\sqrt{6}}(-1, -1, -2), \quad \hat{y}_2 = \frac{1}{\sqrt{2}}(1, -1, 0), \quad \hat{z}_2 = \frac{1}{\sqrt{3}}(-1, -1, 1), \quad (\text{B.2})$$

$$\hat{x}_3 = \frac{1}{\sqrt{6}}(-1, 1, 2), \quad \hat{y}_3 = \frac{1}{\sqrt{2}}(1, 1, 0), \quad \hat{z}_3 = \frac{1}{\sqrt{3}}(-1, 1, -1), \quad (\text{B.3})$$

$$\hat{x}_4 = \frac{1}{\sqrt{6}}(1, -1, 2), \quad \hat{y}_4 = \frac{1}{\sqrt{2}}(-1, -1, 0), \quad \hat{z}_4 = \frac{1}{\sqrt{3}}(1, -1, -1). \quad (\text{B.4})$$

Now, if we have a vector quantity \vec{v}_i that is represented in the local axes at the i^{th} as

$$\vec{v}_i = v_{ix}\hat{x}_i + v_{iy}\hat{y}_i + v_{iz}\hat{z}_i. \quad (\text{B.5})$$

In the global frame this quantity is expressed as $\vec{v}_i = V_i^x \hat{X} + V_i^y \hat{Y} + V_i^z \hat{Z}$, where

$$\begin{pmatrix} V_i^x \\ V_i^y \\ V_i^z \end{pmatrix} = R_i \begin{pmatrix} v_{ix} \\ v_{iy} \\ v_{iz} \end{pmatrix}, \quad (\text{B.6})$$

and $R_i = [\hat{x}_i; \hat{y}_i; \hat{z}_i]$. For example, at site #1, we have

$$R_1 = \begin{pmatrix} \frac{1}{\sqrt{6}} & -\frac{1}{\sqrt{2}} & \frac{1}{\sqrt{3}} \\ \frac{1}{\sqrt{6}} & \frac{1}{\sqrt{2}} & \frac{1}{\sqrt{3}} \\ -\frac{2}{\sqrt{6}} & 0 & \frac{1}{\sqrt{3}} \end{pmatrix}. \quad (\text{B.7})$$

Note that all of the R_i are orthogonal, thus $R_i^{-1} = R_i^T$.

Appendix C

The Eigenvalues and the Eigenvectors of R

The matrix R which appears in Eq. 3.22 is

$$R = \begin{pmatrix} 0 & \cos\left(\frac{1}{4}a(k_x + k_y)\right) & \cos\left(\frac{1}{4}a(k_x + k_z)\right) & \cos\left(\frac{1}{4}a(k_y + k_z)\right) \\ \cos\left(\frac{1}{4}a(k_x + k_y)\right) & 0 & \cos\left(\frac{1}{4}a(k_y - k_z)\right) & \cos\left(\frac{1}{4}a(k_x - k_z)\right) \\ \cos\left(\frac{1}{4}a(k_x + k_z)\right) & \cos\left(\frac{1}{4}a(k_y - k_z)\right) & 0 & \cos\left(\frac{1}{4}a(k_x - k_y)\right) \\ \cos\left(\frac{1}{4}a(k_y + k_z)\right) & \cos\left(\frac{1}{4}a(k_x - k_z)\right) & \cos\left(\frac{1}{4}a(k_x - k_y)\right) & 0 \end{pmatrix}. \quad (\text{C.1})$$

The four eigenvalues of R are

$$r_1 = r_2 = -1, \quad r_{3,4} = r_{\pm} = 1 \pm \alpha(k_x, k_y, k_z), \quad (\text{C.2})$$

where the function $\alpha(k_x, k_y, k_z)$ is

$$\alpha(k_x, k_y, k_z) = \sqrt{1 + \cos\left(\frac{ak_x}{2}\right) \left[\cos\left(\frac{ak_y}{2}\right) + \cos\left(\frac{ak_z}{2}\right) \right] + \cos\left(\frac{ak_y}{2}\right) \cos\left(\frac{ak_z}{2}\right)}. \quad (\text{C.3})$$

For the eigenvectors of R , we start with the eigenvectors that corresponds to $r_{1,2} = -1$ which are

$$\vec{u}_1 = \begin{pmatrix} \frac{1}{2} \csc^2 \left(\frac{1}{4} a (k_x + k_y) \right) \left(\cos \left(\frac{1}{4} a (2k_x + k_y - k_z) \right) - \cos \left(\frac{1}{4} a (k_y + k_z) \right) \right) \\ \frac{1}{2} \csc^2 \left(\frac{1}{4} a (k_x + k_y) \right) \left(\cos \left(\frac{1}{4} a (k_x + 2k_y + k_z) \right) - \cos \left(\frac{1}{4} a (k_x - k_z) \right) \right) \\ 0 \\ 1 \end{pmatrix}, \quad (\text{C.4})$$

$$\vec{u}_2 = \begin{pmatrix} \frac{1}{2} \csc^2 \left(\frac{1}{4} a (k_x + k_y) \right) \left(\cos \left(\frac{1}{4} a (k_x + 2k_y - k_z) \right) - \cos \left(\frac{1}{4} a (k_x + k_z) \right) \right) \\ \frac{1}{2} \csc^2 \left(\frac{1}{4} a (k_x + k_y) \right) \left(\cos \left(\frac{1}{4} a (2k_x + k_y + k_z) \right) - \cos \left(\frac{1}{4} a (k_y - k_z) \right) \right) \\ 1 \\ 0 \end{pmatrix}. \quad (\text{C.5})$$

Note that the above vectors are not orthogonal as they correspond to the same eigenvalue. However, they can be made orthonormal by following the Gram-Schmidt orthonormalization process giving

$$\vec{u}_1 = \frac{\vec{u}_1}{\|\vec{u}_1\|}, \quad \vec{u}_2 = \frac{\vec{u}_2 - \frac{u_1^T u_2}{u_1^T u_1} \vec{u}_1}{\|\vec{u}_2 - \frac{u_1^T u_2}{u_1^T u_1} \vec{u}_1\|}. \quad (\text{C.6})$$

For the r_+ eigenvalue, the corresponding eigenvector is

$$\vec{u}_+ = \begin{pmatrix} a_+ \\ b_+ \\ c_+ \\ 1 \end{pmatrix}, \quad (\text{C.7})$$

where

$$a_+(k) = \frac{2 \sec \left(\frac{1}{4} a (k_y + k_z) \right) \sigma_+^a}{\lambda_+^a}, \quad (\text{C.8})$$

$$\begin{aligned} \sigma_+^a &= \cos \left(\frac{1}{2} a (k_x + k_y) \right) (r_+ + 2) + (r_+ - 1) \left(\cos \left(\frac{1}{2} a (k_x + k_z) \right) + \cos \left(\frac{1}{2} a (k_y + k_z) \right) \right) \\ &+ 5(r_+ - 1) + \cos \left(\frac{1}{2} a (k_x - k_y) \right) + \cos \left(\frac{1}{2} a (k_x - k_z) \right) + 3 \cos \left(\frac{1}{2} a (k_x + k_z) \right) \\ &+ \cos \left(\frac{1}{2} a (k_y - k_z) \right) + 3 \cos \left(\frac{1}{2} a (k_y + k_z) \right) + 4, \end{aligned} \quad (\text{C.9})$$

$$\begin{aligned}
\lambda_+^a = & 14 - 4 \cos^2 \left(\frac{1}{4} a (k_y - k_z) \right) + 4 \cos \left(\frac{ak_y}{2} \right) \cos \left(\frac{ak_z}{2} \right) + 4 \cos \left(\frac{ak_x}{2} \right) \left(\cos \left(\frac{ak_y}{2} \right) + \cos \left(\frac{ak_z}{2} \right) \right) \\
& + 8 (r_+ - 1) + \text{Sec} \left(\frac{1}{4} a (k_y + k_z) \right) \left\{ \cos \left(\frac{1}{4} a (k_y - 3k_z) \right) + 4 \cos \left(\frac{1}{4} a (2k_x + k_y - k_z) \right) \right. \\
& \quad \left. + \cos \left(\frac{1}{4} a (3k_y - k_z) \right) + 4(r_+ - 1) \left[\cos \left(\frac{1}{4} a (k_x + k_y) \right) \cos \left(\frac{1}{4} a (k_x - k_z) \right) \right. \right. \\
& \quad \left. \left. + \cos \left(\frac{1}{4} a (k_y - k_x) \right) \cos \left(\frac{1}{4} a (k_x + k_z) \right) \right] + 4 \cos \left(\frac{1}{4} a (2k_x - k_y + k_z) \right) \right\}, \quad (\text{C.10})
\end{aligned}$$

$$b_+ = \frac{2\sigma_+^b}{\lambda_+^b}, \quad (\text{C.11})$$

$$\begin{aligned}
\sigma_+^b = & 2 \cos \left(\frac{1}{4} a (k_x + k_y) \right) \left[2 - \cos^2 \left(\frac{1}{4} a (k_y - k_x) \right) + \cos \left(\frac{ak_y}{2} \right) \cos \left(\frac{ak_z}{2} \right) + \cos \left(\frac{ak_x}{2} \right) \times \right. \\
& \left. \cos \left(\frac{ak_y}{2} \right) + \cos \left(\frac{ak_z}{2} \right) + 2(r_+ - 1) \right] + \cos \left(\frac{1}{4} a (k_y - k_z) \right) \cos \left(\frac{1}{4} a (k_x + k_z) \right) \times \\
& \left[(1 + 2r_+) + \cos \left(\frac{1}{4} a (k_y + k_z) \right) \left[\cos \left(\frac{1}{4} a (k_x - k_z) \right) (1 + 2r_+) + \cos \left(\frac{1}{4} a (k_x - 2k_y + k_z) \right) \right] \right. \\
& \quad \left. + \cos \left(\frac{1}{4} a (k_x + k_z) \right) \cos \left(\frac{1}{4} a (-2k_x + k_y + k_z) \right) \right], \quad (\text{C.12})
\end{aligned}$$

$$\begin{aligned}
\lambda_+^b = & \cos \left(\frac{1}{4} a (2k_x - 3k_y - k_z) \right) + 6 \cos \left(\frac{1}{4} a (2k_x - k_y + k_z) \right) + \cos \left(\frac{1}{4} a (2k_x - k_y - 3k_z) \right) \\
& + \cos \left(\frac{1}{4} a (3k_y - k_z) \right) + 13 \cos \left(\frac{1}{4} a (k_y + k_z) \right) + \cos \left(\frac{1}{4} a (k_y - 3k_z) \right) \\
& 2 \cos \left(\frac{1}{4} a (2k_x + k_y - k_z) \right) (2 + r_+) + 2(r_+ - 1) \left(\cos \left(\frac{1}{4} a (2k_x - k_y + k_z) \right) + 6 \cos \left(\frac{1}{4} a (k_y + k_z) \right) \right) \\
& \cos \left(\frac{1}{4} a (2k_x + 3k_y + k_z) \right) + \cos \left(\frac{1}{4} a (2k_x + k_y + 3k_z) \right) + \cos \left(\frac{3}{4} a (k_y + k_z) \right), \quad (\text{C.13})
\end{aligned}$$

and,

$$c_+ = -\frac{\sigma_+^c}{\lambda_+^c}, \quad (\text{C.14})$$

$$\begin{aligned} \sigma_+^c = & \frac{1}{2} \cos\left(\frac{ak_y}{2} - \cos\left(\frac{ak_x}{2}\right)\right) \left[r_+ \cos\left(\frac{1}{4}a(k_x + k_y)\right) + \cos\left(\frac{1}{4}a(k_x - k_z)\right) \cos\left(\frac{1}{4}a(k_y + k_z)\right) \right] \\ & - \cos\left(\frac{1}{4}a(k_y - k_x)\right) \cos\left(\frac{1}{4}a(k_y + k_z)\right) - r_+ \cos\left(\frac{1}{4}a(k_x + k_z)\right) - r_+ \cos\left(\frac{1}{4}a(k_y + k_z)\right) \\ & - \cos\left(\frac{1}{4}a(k_x + k_y)\right) \cos\left(\frac{1}{4}a(k_x - k_z)\right), \end{aligned} \quad (\text{C.15})$$

$$\begin{aligned} \lambda_+^c = & \frac{1}{4} \left(\cos\left(\frac{ak_x}{2}\right) - \cos\left(\frac{ak_y}{2}\right) \right) \left(\cos\left(\frac{ak_x}{2}\right) - \cos\left(\frac{ak_z}{2}\right) \right) \\ & + \cos\left(\frac{1}{4}a(k_x + k_y)\right) \cos\left(\frac{1}{4}a(k_x - k_z)\right) + r_+ \cos\left(\frac{1}{4}a(k_y + k_z)\right) \\ & - \cos\left(\frac{1}{4}a(k_y - k_x)\right) \cos\left(\frac{1}{4}a(k_x + k_z)\right) - r_+ \cos\left(\frac{1}{4}a(k_y + k_z)\right). \end{aligned} \quad (\text{C.16})$$

Finally, the last eigenvector which corresponds to the eigenvalue r_- is

$$\vec{u}_- = \begin{pmatrix} a_- \\ b_- \\ c_- \\ 1 \end{pmatrix}, \quad (\text{C.17})$$

where

$$a_-(k) = \frac{2 \sec\left(\frac{1}{4}a(k_y + k_z)\right) \sigma_-^a}{\lambda_-^a}, \quad (\text{C.18})$$

$$\begin{aligned} \sigma_-^a = & -\cos\left(\frac{1}{2}a(k_x + k_y)\right) (r_- + 2) + (1 - r_-) \left(\cos\left(\frac{1}{2}a(k_x + k_z)\right) + \cos\left(\frac{1}{2}a(k_y + k_z)\right) \right) \\ & + 5(1 - r_-) - \cos\left(\frac{1}{2}a(k_x - k_y)\right) - \cos\left(\frac{1}{2}a(k_x - k_z)\right) - 3 \cos\left(\frac{1}{2}a(k_x + k_z)\right) \\ & + \cos\left(\frac{1}{2}a(k_y - k_z)\right) - 3 \cos\left(\frac{1}{2}a(k_y + k_z)\right) - 4, \end{aligned} \quad (\text{C.19})$$

$$\lambda_-^a = -6 - 2 \cos\left(\frac{ak_y}{2}\right) \cos\left(\frac{ak_z}{2}\right) + 6(1 - r_-) - 2 \cos\left(\frac{ak_x}{2}\right) \times$$

$$\left[(r_- + 1) \cos\left(\frac{1}{4}a(k_y - k_z)\right) \sec\left(\frac{1}{4}a(k_y + k_z)\right) + \cos\left(\frac{ak_y}{2}\right) + \cos\left(\frac{ak_z}{2}\right) \right] \quad (\text{C.20})$$

$$b_- = \frac{4\sigma_-^b}{\lambda_-^b}, \quad (\text{C.21})$$

$$\begin{aligned} \sigma_-^b = & \cos\left(\frac{1}{4}a(k_x + k_y)\right) \left[\cos\left(\frac{ak_x}{2}\right) \left(\cos\left(\frac{ak_y}{2}\right) + \cos\left(\frac{ak_z}{2}\right) \right) - \cos^2\left(\frac{1}{4}a(k_y - k_x)\right) \right. \\ & \left. + \cos\left(\frac{ak_y}{2}\right) \cos\left(\frac{ak_z}{2}\right) - 2(1 - r_-) + 2 \right] + \frac{1}{2}(1 - 2r_-) \cos\left(\frac{1}{4}a(k_x + k_z)\right) \cos\left(\frac{1}{4}a(k_y - k_z)\right) \\ & \frac{1}{2} \left[\cos\left(\frac{1}{4}a(k_y + k_z)\right) \left((1 - r_-) \cos\left(\frac{1}{4}a(k_x - k_z)\right) + \cos\left(\frac{1}{4}a(k_x - 2k_y + k_z)\right) \right) \right. \\ & \left. + \cos\left(\frac{1}{4}a(k_x + k_z)\right) \cos\left(\frac{1}{4}a(-2k_x + k_y + k_z)\right) \right], \quad (\text{C.22}) \end{aligned}$$

$$\begin{aligned} \lambda_-^b = & \cos\left(\frac{1}{4}a(2k_x - 3k_y - k_z)\right) + 6 \cos\left(\frac{1}{4}a(2k_x - k_y + k_z)\right) + \cos\left(\frac{1}{4}a(2k_x - k_y - 3k_z)\right) \\ & + \cos\left(\frac{1}{4}a(3k_y - k_z)\right) + 13 \cos\left(\frac{1}{4}a(k_y + k_z)\right) + \cos\left(\frac{1}{4}a(k_y - 3k_z)\right) + 2 \times \left[\right. \\ & \left. (r_- + 1) \cos\left(\frac{1}{4}a(2k_x + k_y - k_z)\right) - (r_- - 1) \left(\cos\left(\frac{1}{4}a(2k_x - k_y + k_z)\right) + 6 \cos\left(\frac{1}{4}a(k_y + k_z)\right) \right) \right] \\ & + \cos\left(\frac{1}{4}a(2k_x + 3k_y + k_z)\right) + \cos\left(\frac{1}{4}a(2k_x + k_y + 3k_z)\right) + \cos\left(\frac{3}{4}a(k_y + k_z)\right), \quad (\text{C.23}) \end{aligned}$$

and,

$$c_- = \frac{\sigma_-^c}{\lambda_-^c}, \quad (\text{C.24})$$

$$\sigma_-^c = -2(r_- - 1) \cos\left(\frac{1}{4}a(k_x + k_z)\right) + \cos\left(\frac{1}{4}a(k_x + 2k_y - k_z)\right) + \cos\left(\frac{1}{4}a(k_x - 2k_y - k_z)\right), \quad (\text{C.25})$$

$$\lambda_-^c = -2(r_- - 1) \cos\left(\frac{1}{4}a(k_y + k_z)\right) + \cos\left(\frac{1}{4}a(2k_x + k_y - k_z)\right) + \cos\left(\frac{1}{4}a(2k_x - k_y + k_z)\right). \quad (\text{C.26})$$

Thus, we have now extracted the set of eigenvalues and the corresponding eigenvectors of R which will be used to construct the exact energy dispersions and the Bogoliubov matrix for the AIAO ground state in the $\Gamma_{5,6}$ pyrochlores.

Appendix D

Analytic Solutions of the Quartic Equation

Defining $x(k) = \varepsilon^2(k)$, Eq. (4.6) results in a quartic equation in x with real coefficients,

$$x^4 + \xi_6(k)x^3 + \xi_4(k)x^2 + \xi_2(k)x + \xi_0(k) = 0. \quad (\text{D.1})$$

The four roots of Eq. (D.1) are

$$x = -\frac{\xi_6(k)}{4} \pm \mathcal{S}(k) \pm \frac{1}{2} \sqrt{-4\mathcal{S}^2(k) - 2P(k) \mp \frac{Q(k)}{\mathcal{S}(k)}}, \quad (\text{D.2})$$

where $P(k) = \xi_4(k) - \frac{3}{8}\xi_6^2(k)$, $Q(k) = \xi_2(k) - \frac{1}{2}\xi_6(k)\xi_4(k) + \frac{1}{8}\xi_6^3(k)$, and

$$\mathcal{S}(k) = \frac{1}{2} \sqrt{-\frac{2}{3}P(k) + \frac{1}{3} \left(T(k) + \frac{\Delta_0(k)}{T(k)} \right)}, \quad (\text{D.3})$$

with $\Delta_0(k) = \xi_4^2(k) - 3\xi_6(k)\xi_2(k) + 12\xi_0(k)$ and

$$T(k) = \sqrt[3]{\frac{\Delta_1 + \sqrt{\Delta_1^2 - 4\Delta_0^3}}{2}}, \quad (\text{D.4})$$

,

$$\Delta_1 = 2\xi_4^3 - 9\xi_6(k)\xi_4(k)\xi_2(k) + 27\xi_6^2(k)\xi_0(k) + 27\xi_2^2(k) - 72\xi_4(k)\xi_0(k). \quad (\text{D.5})$$

We define the discriminant Δ as

$$\Delta = \frac{4\Delta_0^3 - \Delta_1^2}{27}. \quad (\text{D.6})$$

Acceptable physical solutions are non-negative real numbers. In this case, the energy bands of magnons are

$$\varepsilon(k) = \sqrt{-\frac{\xi_6(k)}{4} \pm \mathcal{S}(k) \pm \frac{1}{2} \sqrt{-4\mathcal{S}^2(k) - 2P(k) \mp \frac{Q(k)}{\mathcal{S}(k)}}}. \quad (\text{D.7})$$

Appendix E

Calculations of the BT Matrix Z

We start by rewriting the three conditions that the BT matrix must satisfy at one time,

$$Z^{-1}\mathcal{G}MZ = \begin{pmatrix} \mathcal{E} & 0 \\ 0 & -\mathcal{E} \end{pmatrix}, \quad (\text{E.1})$$

$$Z\mathcal{G}Z^\dagger = \mathcal{G} = \begin{pmatrix} \mathbb{1} & 0 \\ 0 & -\mathbb{1} \end{pmatrix}, \quad (\text{E.2})$$

$$Z^\dagger MZ = \begin{pmatrix} \mathcal{E} & 0 \\ 0 & \mathcal{E} \end{pmatrix}. \quad (\text{E.3})$$

The procedure for finding Z is as follows. We assume that $\mathcal{G}M$ has q distinct eigenvalues (where $q \leq 8$ in our case), each with degeneracy d_i were the eigenvalues of $\mathcal{G}M$ are related to the energy dispersions of magnons through Eq. (E.1). We begin by finding the normalized eigenvectors of $\mathcal{G}M$ and grouping them such that the eigenvectors belonging to the same eigenspace go together. In this case we end up with a matrix of eigenvectors of $\mathcal{G}M$ which we will call \tilde{Z} . Now, finding the BT matrix Z can be done by introducing a block diagonal transformation P such that $Z = \tilde{Z}P$. The sizes of the blocks of P are $d_i \times d_i$ and the number of blocks is at most 8 in our case. The matrix Z is basically found by some linear combinations of the eigenvectors of $\mathcal{G}M$ each within the same given eigenspace, which means that Z satisfies Eq. (E.1). For Z to satisfy Eq. (E.2), we must have

$$P\mathcal{G}P^\dagger = (\tilde{Z}^\dagger\mathcal{G}\tilde{Z})^{-1}. \quad (\text{E.4})$$

Now, we come to the importance of organizing the eigenvectors. The Hermitian matrix $W = (\tilde{Z}^\dagger \mathcal{G} \tilde{Z})^{-1}$ will have block form with q blocks each with dimension $d_i \times d_i$. Considering block by block, we arrive at the following equation

$$\pm P_i P_i^\dagger = W_i, \quad (\text{E.5})$$

where the \pm sign related to whether we are in the positive or negative energy sector of $\mathcal{G}M$. Since the block W_i is Hermitian, we can write it in terms of unitary matrix X_i as follows [47]

$$W_i = X_i D_i X_i^{-1}, \quad (\text{E.6})$$

where D_i is the diagonal matrix containing the eigenvalues of W_i . Consequently, the solution of P_i is given below

$$P_i = X_i \sqrt{\pm D_i} X_i^{-1}, \quad (\text{E.7})$$

where P_i can be found either analytically or numerically depending on the possible analytic calculations of X_i . Thus, we have now constructed the full BT matrix Z which satisfies Eqs. (E.1) and (E.2). Obviously, Eq. (E.3) is automatically satisfied. Note that this procedure is suitable for all cases when no Goldstone mode appears. This case must be treated separately as special cases. With the models we studied, gapless excitations only appear in $\text{Er}_2\text{Ti}_2\text{O}_7$ at the Γ point. In this case, the Γ point can be studied separately. We have used Mathematica to do the diagonalization of the various Hamiltonians and obtaining the energy dispersions for each case.